Fungal Genetics and Biology 162 (2022) 103729

Contents lists available at ScienceDirect

Fungal Genetics and Biology

journal homepage: www.elsevier.com/locate/yfgbi

The cytoplasmic microtubule array in *Neurospora crassa* depends on microtubule-organizing centers at spindle pole bodies and microtubule +end-depending pseudo-MTOCs at septa

Rosa Ramírez-Cota [a], Astrid N. Espino-Vazquez [a], Tonacy C. Rodriguez-Vega [a], Rocío E. Macias-Díaz [a], Olga A. Callejas-Negrete [a], Michael Freitag [b], Reinhard Fischer [c], Robert W. Roberson [d], Rosa R. Mouriño-Pérez [a,*]

[a] Departamento de Microbiología. Centro de Investigación Científica y de Educación Superior de Ensenada (CICESE), Ensenada, B.C., Mexico
[b] Department of Biochemistry and Biophysics, Center for Genome Research and Biocomputing, Oregon State University, Corvallis, OR, USA
[c] Department of Microbiology, Institute for Applied Biosciences, Karlsruhe Institute of Technology (KIT), South Campus, Fritz-Haber-Weg 4, Karlsruhe D-76131, Germany
[d] School of Life Sciences, Arizona State University, Tempe, AZ, USA

ARTICLE INFO

Keywords:
Neurospora crassa
Microtubules
MTOCs
Spindle pole bodies
γ-Tubulin
PCP-1
Aps-2
SPA10
SPA-18
MTB-3

ABSTRACT

γ-Tubulin ring complexes (γ-TuRC) mediate nucleation and anchorage of microtubules (MTs) to microtubule organizing centers (MTOCs). In fungi, the spindle pole body (SPB) is the functional equivalent of the centrosome, which is the main MTOC. In addition, non-centrosomal MTOCs (ncMTOCs) contribute to MT formation in some fungi like *Schizosaccharomyces pombe* and *Aspergillus nidulans*. In *A. nidulans,* MTOCs are anchored at septa (sMTOC) and share components of the outer plaque of the SPB. Here we show that the *Neurospora crassa* SPB is embedded in the nuclear envelope, with the γ-TuRC targeting proteins PCP-1$^{Pcp1/PcpA}$ located at the inner plaque and APS-2$^{Mto1/ApsB}$ located at the outer plaque of the SPB. PCP-1 was a specific component of nuclear MTOCs, while APS-2 was also present at the septal pore. Although γ-tubulin was only detected at the nucleus, spontaneous MT nucleation occurred in the apical and subapical cytoplasm during recovery from benomyl-induced MT depolymerization experiments. There was no evidence for MT nucleation at septa. However, without benomyl treatment MT plus-ends were organized in the septal pore through MTB-3^{EB1}. Those septal MT plus ends polymerized MTs from septa in interphase cells Thus we conclude that the SPB is the only MT nucleation site in *N. crassa*, but the septal pore aids the MT network arrangement through the anchorage of the MT plus-ends through a pseudo-MTOC.

1. Introduction

γ-tubulin is the major microtubule (MT) nucleator at MT-organizing centers (MTOCs) and was discovered in *Aspergillus nidulans* in 1989 (Oakley and Oakley, 1989). It is a member of the tubulin family sharing 35% identity with α/β- tubulin and is highly conserved among eukaryotic organisms (Horio and Oakley, 2003; Horio et al., 1991; Julian et al., 1993; Liu et al., 1994). γ-Tubulin is associated with other *Gamma Tubulin Complex Proteins* (GCPs in humans) to form different γ-tubulin complexes (γ-TuCs). In *Saccharomyces cerevisiae,* γ-tubulin, together with Spc97 (GCP2) and Spc98 (GCP3), form the so-called γ-tubulin small complex (γ-TuSC) (Kollman et al., 2010; Moritz et al., 2000). The γ-TuSC nucleates MTs and thereby provides a template for the assembly of α/β-tubulin heterodimers (Kollman et al., 2011; Oakley et al., 2015; Teixidó-Travesa et al., 2012). In the fission yeast *Schizosaccharomyces pombe* and higher eukaryotes, the γ-TuC may contain additionally GCP4, GCP5, and GCP6 and a small protein called Mozart (Mzt1) (Cota et al., 2017; Lin et al., 2016; Lin et al., 2014; Teixidó-Travesa et al., 2012). Recently, cryoelectron microscopy reconstructions identified actin as a new constituent of vertebrate γ-TuRC (Liu et al., 2021; Liu et al., 2020; Zupa et al., 2021). However, γ-TuC composition appears to be more diverse in fungi as *Candia albicans* contains γ-TuSCs with the additional Mozart protein (Lin et al., 2016). γ-TuCs are organized in higher-ordered protein complexes, the MTOCs (Horio et al., 1991; Liu et al., 1993;

* Corresponding author.
E-mail address: rmourino@cicese.mx (R.R. Mouriño-Pérez).

https://doi.org/10.1016/j.fgb.2022.103729
Received 18 April 2022; Received in revised form 22 July 2022; Accepted 25 July 2022
Available online 6 August 2022

Muresan et al., 1993; Oakley and Oakley, 1989; Stearns et al., 1991; Zheng et al., 1991). In most animal cells, γ-tubulin is associated with the centrosomes, and in fungal cells, it is associated with its functional counterpart, the spindle pole body (SPB) (Khodjakov and Rieder, 1999; Lajoie-Mazenc et al., 1994). Both centrosomes and SPBs organize the mitotic spindle.

Most fungal γTuC proteins are evolutionarily conserved (Table 1), and the yeast *S. cerevisiae* SPB is among the best-characterized MTOCs (Cavanaugh and Jaspersen, 2017; Kilmartin, 2014; Snyder, 1994). It is embedded into the nuclear envelope and composed of three layers, an outer plaque facing the cytoplasm, a central plaque anchored at the nuclear envelope, and an inner plaque facing the nucleoplasm (Jaspersen and Winey, 2004). At the outer plaque of the SPB, γ-TuSCs are recruited by Spc72 (Knop and Schiebel, 1997), whereas at the inner plaque, Spc110 is the γTuSC receptor (Kollman et al., 2010). The CM1 (centrosomin motif) and SPM motif (Spc110/Pcp1 motif) of Spc110 interact directly with the N-terminus of GCP3 and possibly of GCP2 (Knop and Schiebel, 1997; Kollman et al., 2010; Lin et al., 2016; Lin et al., 2014). In contrast to *S. cerevisiae*, *S. pombe* possesses γTuRCs with γ- tubulin and GCP4-6 and Mzt1 orthologs at the inner and the outer plaque (Anders et al., 2006; Dhani et al., 2013; Fujita et al., 2002; Lin et al., 2015; Masuda et al., 2013). This process resembles the recruitment in *S. cerevisiae* with Pcp1 (Spc110 orthologue) as a receptor at the inner plaque and Mto1 (Spc72 orthologue) at the outer plaque. However, Mto1 requires a second receptor protein, Mto2, to activate MT nucleation (Lynch et al., 2014; Samejima et al., 2008; Samejima et al., 2010). In *A. nidulans,* the situation is even more complex because it harbors both γTuSCs and TuRCs (Gao et al., 2019; Xiong and Oakley, 2009). γ-Tubulin complexes are characteristic of the outer and the inner plaques, respectively, γTuSCs are recruited to the outer plaque of the SPBs by ApsB^{Mto1} and Spa18^{Mto2}, and γTuRCs, including the Mozart protein MztA, to the inner plaque by PcpA^{Pcp1} (Gao et al., 2019; Zhang et al., 2017).

In addition to centrosomes and SPBs, non-centrosomal MTOCs (ncMTOCs) have been identified in different organisms. In animal cells, MTs appear to be nucleated from the Golgi (Chabin-Brion et al., 2001; Maia et al., 2013; Paz and Lüders, 2018; Rivero et al., 2009; Zimmerman et al., 2004), and during mitosis, MTs are also nucleated and organized at the kinetochores and from pre-existing MTs within the spindle (Kaláb et al., 2006; Maiato et al., 2004). Plants lack centrosomes, but γ-tubulin is associated with all MT arrays and the nuclear membrane (A.C., 2002; Lee and Liu, 2019; Yi and Goshima, 2018). In fungi, ncMTOCs have been described as being associated with the Spitzenkörper (Spk) in *Allomyces macrogynus* (McDaniel and Roberson, 1998), the cytoplasm in interphase, and the equatorial plate during mitosis in *Ustilago maydis,* and *S. pombe* (Bartolini and Gundersen, 2006; Horio et al., 1991; Lin et al., 2015; Straube et al., 2003), or at septa in *A. nidulans* (Konzack et al., 2005; Oakley, 2004; Oakley and Oakley, 1989; Zekert et al., 2010; Zhang et al., 2017). Understanding the organization and functioning of fungal ncMTOCs is still in its infancy. In *A. nidulans,* septal MTOCs contain γTuRCs with MztA, but they are anchored at septa by ApsB and Spa18 and the intrinsically disordered protein, Spa10 (Zhang et al., 2017). Hence, *A. nidulans* contains three different γTuCs, γTuSCs (with ApsB and Spa18 as receptors), γTuRCs with MztA (with PcpA as a receptor). Recently, it was shown that the activity of the sMTOCs and the outer plaque of the SPBs are coordinately regulated through a polo-like kinase, PlkA (Gao et al., 2021).

In *N. crassa,* the cellular and cytoskeletal organization is very different from the organization in *S. pombe*, *C. albicans,* or *A. nidulans*. Whereas hyphae of *A. nidulans* contain 3-6 nuclei, the hyphae of *N. crassa* are much wider, and each compartment contains ~100 nuclei, from where cytoplasmic MTs polymerize (Roper et al., 2011; Fischer & Timberlake, 1995). Whereas MTs in *A. nidulans* appear oriented along the long axis of the hyphae, MTs in *N. crassa* are much more chaotic but converge at the Spk. There are instances of MT polymerization from the apical dome suggesting the existence of ncMTOC at the hyphal apex (Mouriño-Pérez et al., 2006; Uchida et al., 2008). In addition, there is an accumulation of the MT plus end protein MTB-3 (EB1 homolog) at the septal pore, where MTs form a bundle (Mouriño-Pérez et al., 2013). However, it remained to be established whether ncMTOCs are found at the Spk and/or septa. In this study, we combined live-cell imaging of strains with fluorescently tagged MTOC proteins and proteomic approaches to determine the localization and composition of the γ-tubulin-dependent MTOCs in *N. crassa*. We show that PCP-1$^{Pcp1/PcpA}$ and APS-2$^{Mto1/ApsB}$ co-localize with γ-tubulin at the inner and outer plaque of the SPB, respectively, where MTs are nucleated. Besides the polymerization of MTs from SPBs, MT formation spontaneously occurred at the apical and subapical cytoplasm. Although Aps-2 localized at septal pores, there was no evidence for active septal MTOCs. In contrast, MTs from adjacent compartments squeezed through the pores and formed aster-like MT arrays. Here we show that SPA10 and APS-2/SPA-18 associated with MTB-3 are necessary for the organization of the MT-plus end to the septal pore but not for MT nucleation.

Table 1
Known fungal MTOC components and predicted homologs in *N. crasssa*.

S. cerevisiae	*A. gossypii*	*C. albicans*	*S. pombe*	*A. nidulans*	*N. crassa*/Accession
Tub4	Tub4	Tub4	Gtb1	MipA*	γ-Tubulin/NCU03954
Spc97	Spc97	Spc97	Alp4	GcpB*	GCP-2/NCU05296
Spc98	Spc98	Spc98	Alp6	GcpC*	GCP-3/NCU04319
-	-	-	Gfh1	GcpD*	GCP-4/NCU06988
-	-	-	Mod21	GcpE*	GCP-5/NCU01387
-	-	-	Alp16	GcpF*	GCP-6/NCU05282
-	-	Mzt1	Mzt1	MztA*	MZT-1/NCU11158
Stu2	Stu2	Stu2	Alp14	AlpA	ALP-1/NCU04535
Spc110	Spc110	Spc110	Pcp1	PcpA	PCP-1/NCU02411
Spc72	Spc72	Spc72	Mto1	ApsB*	APS-2/NCU17239
-	-	-	-	Spa10*	SPA10/ NCU04258
-	-	-	Mto2	Spa18*	SPA18/NCU06253
Cmd1	Cmd1	Cmd1	Cam1	Calmodulin	CMD-1/NCU04120
Spc42	Spc42	-	-	-	-
Spc29	Spc29	-	-	-	-
Cnm67	Cnm67	Cnm67	Sid4	-	-
Nud1	Nud1	Nud1	Cdc11	SepK	CDC-11/NCU03545?
Sfi1	Sfi1	Sfi1	Sfi1	SfiA	SFI-1/NCU03573
Cdc31	Cdc31	Cdc31	Cdc31	Cdc31	CDC-31/NCU09871
Kar1	Kar1	-	-	-	-
Mps2	Mps2	-	Kms2	-	-
Ndc1	Ndc1	Ndc1	Cut11	Ndc1	NDC-1/NCU06776

*Proposed cnMTOC component in *A. nidulans* {1}{2}

2. Material and methods

2.1. Strains and culture conditions

The strains used in this study are listed in Table 2. Strains were maintained at 30 °C on Vogel's minimal media (VMM) (Vogel, 1956) with 1.5% sucrose and 1.5% agar. All manipulations were according to standard techniques (Davis and Perkins, 2002).

2.2. Constructions of plasmids containing γ-tubulin, pcp-1, aps-2, and mzt-1 genes fusion expressing tagged fluorescent protein

The *N. crassa tbg* (NCU03954), *pcp-1* (NCU02411), *aps-2* (NCU04258), and *mzt-1* (KHE87685.1) genes were identified by BLASTP search at FungiDB Fungal and Oomycete Genomics Resources database (https://fungidb.org/fungidb/). Standard PCR and cloning procedures (Sambrook J. et al., 1989) were used to fuse the *sgfp* gene to the end of the *tbg, pcp-1,* and *mzt-1* genes, and *drfp* to the beginning of *aps-2*. The open reading frame (ORF) of the genes was amplified by PCR from *N. crassa* (FGSC2489) genomic DNA. Primers and plasmids used are listed in Table 2. PCR was performed in an Apollo Thermal Cycler (Thermo Fisher Scientific Inc.) with Phusion High-Fidelity DNA Polymerase (New England Biolabs Inc.) according to the manufactureŕs instructions. The *tbg* gene was amplified with the primers TBGF and TBGR, *pcp-1* gene was amplified with the primers GRBxbaF and GRBpacR, *mzt-1* gene was amplified whit the primers MztXbaIF and MztPacIR and *aps-2* gene was amplified with the primers N-Aps1-SpeI-F and Aps-1-FseI-NG-R. The amplified PCR products were gel purified, and *tbg, pcp-1, mzt-1* were digested with XbaI and PacI and ligated into XbaI- and PacI-digested plasmid pMF272 (GeneBank accession no. AY598428). This yielded pRM01-RR01(*tbg* -sgfp), pRM61-RR04 (*pcp-1-sgfp*) and pRM99-TR01 (*mzt-1-sgfp*), while *aps-2* was digested with SpeI and FseI and ligated into SpeI- and FseI- digested plasmid pMF336 (Freitag and Selker, 2005) yielding pRM91-RR13 (*drfp-asps-2*).

2.3. Constructions of tbg, pcp-1, mzt-1 and spa-10 genes fusion with fluorescent proteins

The *N. crassa spa-10* (NCU17239) genes were identified by BLASTP search at FungiDB Fungal and Oomycete Genomics Resources database (https://fungidb.org/fungidb/). The construction of the recombinant dsDNA for the "knock-in" technique was achieved by split marker fusion PCR (Sambrook et al., 1989). *tbg, pcp-1, mzt-1* and *spa-10* genes were amplified by PCR from *N. crassa* (FGSC2489) genomic DNA. Primers used are listed in Table 2. PCR was performed in an Apollo Thermal Cycler (Thermo Fisher Scientific Inc.) with Phusion High-Fidelity DNA Polymerase (New England Biolabs Inc.) according to the manufactureŕs instructions. For the C-terminal tagging of *tbg, pcp-1* and *mzt-1* genes with *mchfp* expressed under the native promoter, we used ~1.0 kb from the 3́end of ORF (named 5́fragment), excluding the stop codon, and ~1.0 kb of the 3́UTR (named 3́fragment). The *tbg* 5́fragment was PCR amplified with the primers Tbg5'F and Tbg5'R, and the *tbg* 3́frament was amplified with the primers Tbg3'F and Tbg3'R. For *pcp-1* 5́fragment, the primers GRB5́F and GRB5́R, and the primers GRB3'F and GRB3'R for the 3́fragment were used. For *mzt-1* 5'fragment, the primers MZT1-5'F and MZT1gly-5'R, and the primers MZT1loxp-3'F and MZT1-3'R for the 3́fragment were used. A fragment of *mchfp::hph* was amplified from pRR1-0mChFP using primers GlyF and LoxpR. Subsequently, *mchfp::hph* fragment was fused with the 3́end fragment and with the 3́UTR of the genes by fusion PCR; for *tbg* using primers Tbg5'F and hphSMR and hphSMF and Tbg3'R, for *pcp-1* using primers GRB5'F and hphSMR and hphSMF and GRB3'R and for *mzt-1* using primers MZT1-5'F - hphSMR and hphSMF - MZT1-3'R. The two PCR amplicons were used to replace the 3́end of *tbg*, *pcp-1* or *mzt-1*. For *spa-10* C-terminal tagging with *sgfp* expressed under the native promoter, we used the primers rcSPA10_5F and rcSPA10gly_5R, and the primers rcSPA10loxp_3F and rcSPA10_3R. A fragment of *sgfp*::*hph* was amplified from pZero (Honda and Selker, 2009) using primers GlyF and LoxpR. Subsequently, *sgfp*::*hph* fragment was fused with the 3́end fragment and the 3́UTR of the gene by fusion PCR, using primers rcSPA10_5F and hphSMR and hphSMF and rcSPA10_3R. The two PCR amplicons were used to replace the 3́end of *spa10*.

2.4. Transformation protocols, transformant selection, and crosses

Transformation of N. crassa strain FGSC9717 Δ*mus-51* his-3 conidia with non-linearized plasmids pRM01-RR01, pRM61-RR04, pRM91-RR13, and pRM99-TR01 (Table 2) or with the cassette for the endogenous promotor expression was carried out by electroporation on a Bio-Rad Gene Pulser (Model Xcell) (capacitance, 25 μF; 1.5 kV; resistance, 600 Ω) as previously described (Margolin et al., 1997). By confocal microscopy, Prototrophic His+ or Hygromycin resistance was screened for the expression of GFP, mChFP, or dRFP. Transformant showing fluorescence where selected and named as TRM01-RR01 (*tbg-sgfp*), TRM61-RR04 (*pcp-1-sgfp*), TRM99-TR01 (*mzt-1-sgfp*), TRM100-TR02 (*mzt-1-mchfp*), TRM128-RR10 (*drfp-aps-2*), TRM66-RR07 (*pcp-1-mchfp*), TRM68-RR09 (*tbg-mchfp*) and TRM129-RR11 (*spa-10-sgfp*) (Table 2). The heterokaryon strain selected for each transformation was crossed to obtain a homokaryotic strain. Strains were crossed routinely on synthetic crossing medium (SCM) plates supplemented with 1% sucrose and 2% agar (Davis, 2000). For each cross, the conidia of the first strain were grown on SCM for 5 d at 30°C and then fertilized by adding conidia from the second parent. After 14 d of incubation at 25°C in the dark, ascospores from the developed perithecia were collected from the Petri plate covers with distilled water. Ascospores were spread onto VMM, heat-shocked at 60°C for 60 min, and incubated for 12 h at 30°C. Colonies were transferred to 1 ml culture tubes with VMM and incubated for 24 h at 30°C, and screened to select for GFP, mChFP, or dRFP expression.

2.5. Co-expression assays

To examine the relationship between the different components of the MTOCs and Mts and nuclei, we constructed heterokaryons from two strains of *N. crassa* of the same mating type by vegetatively fusing a strain labeled with mChFP or dRFP with a strain expressing GFP. For each pair of strains, a VMM plate was inoculated with spores of both strains and incubated for 10 h at 28°C. Colonies were screened for hyphae having both fluorescent makers and then carefully imaged following the procedure described for laser scanning confocal microscopy.

2.6. Calcofluor white staining and FM4-64

Calcofluor white (CW) dye was used to visualize the cell wall, and FM4-64 dye was used to visualize the cell membrane, the Spk, and septa. Strains were incubated with 5 μl (5 μM) of FM4-64 (Molecular Probes, Eugene, OR) or with Calcofluor white (Sigma) 5 μl (2 μg ml^{-1}) for 5 min before microscopic analysis using the inverted agar block method (Hickey et al., 2002).

2.7. Microtubule depolymerization assay

A stock solution of benomyl (BML; methyl 1-[butyl-carbamoyl]-2-benz-imidazolecarbamate; Sigma) at 10 mg ml^{-1} was prepared in 100 % ethanol. Serial dilutions of the drug were tested on VMM plates at ten-fold concentration increments (0.01 μg ml^{-1} to 10 μg ml^{-1}). The concentration that inhibited hyphal growth rate by 50% was selected for further studies (0.5 μg ml^{-1}). Thus, to study the effect of the anti-MT drug BML on MTs and γ-tubulin distribution in *N. crassa*, we inoculate conidia of the strain co-expressing the γ-tubulin-mChFP and β-tubulin-GFP on VMM agar (1.5 % sucrose) on top a nitrocellulose membrane and

Table 2
Neurospora crassa strains, plasmids and oligonucleotides used in this study

Name	Genotype	Reference
Strains		
FGSC4200	*mat a Wild type*	FGSC
FGSC9717	*mat A; his-3; Δmus-51::bar+*	FGSC
FGSC9538	*mat a; his-3; Δmus-51::bar+*	FGSC
FGSC2389	*mat A; Δspa-10; hph+*	FGSC
FGSC2390	*mat a; Δspa-10; hph+*	FGSC
FGSC15177	*mat a; Δspa-18; hph+*	FGSC
FGSC15178	*mat A; Δspa-18; hph+*	FGSC
N2282	*mat A; his-3+ ::Pccg-1-h+-sgfp+*	Freitag et al. 2004
NMF138	*mat A; his-3+ ::Pccg-1-h1-drfp+*	Freitag et al. 2004
N2526	*mat A; ridRIP1; his-3+::Pccg-1-bml-sgfp+*	Freitag et al. 2004
TRM19-OC12	*mat A; his-3+ ::Pccg-1-bml-mchfp+*	Callejas-Negrete et al. 2015
XTL2-1	*mat A; his-3+::Pccg-1-mtb-3-sgfp+*	Mouriño-Pérez et al. 2013
TRM02-AR	*mat A; his-3+::Pccg-1-mtb-3-mchfp+*	Mouriño-Pérez et al. 2013
NMF556	*mat a; his-3+ ::Pccg-1-son-1-sgfp+*	Freitag et al.
NMF557	*mat A; his-3+ ::Pccg-1-son-1-sgfp+*	Freitag et al.
TRM47-OC28	*mat a; his-3+ ::Pccg-1-tpm-1 -sgfp+*	Delgado-Alvarez et al. 2010
TRM01-RR01	*mat a; his-3+ ::Pccg-1-tbg-sgfp+*	This study
TRM61-RR04	*mat a; his-3+ ::Pccg-1-pcp-1-sgfp+*	This study
TRM66-RR07	*mat a; his-3::Ppcp-1-pcp-1-mchfp+; hph+*	This study
TRM68-RR09	*mat a; his-3+::Ptbg-tbg-mCHFP; hph+*	This study
TRM99-TR01	*mat A; his-3+::Pccg-1-mzt-1-sgfp+*	This study
TRM100-TR02	*mat A; his-3::Pmzt-1-mzt-1-mchfp hph+*	This study
TRM128-RR10	*mat A; his-3+::Pccg-1-drfp+-aps-2*	This study
TRM129-RR11	*mat a; his-3::Pspa-10-spa-10-sgfp+; hph+*	This study
TRM132-RR14	*mat A; his-3+::Pccg1-mtb-3-mchfp+ ; Pspa-10-spa-10-sgfp+; hph+*	This study
TRM134-RR16	*mat A; his-3+:: Pccg1-mtb-3-sgfp+; Δspa-10; hph+*	This study
TRM135-RR17	*mat A; his-3+:: Pccg1-mtb-3-sgfp+; Δspa-18; hph+*	This study
TRM136-RR18	*Mat a; his-3+::Pccg-1-bml-sgfp+; Ptbg-tbg-mchfp+; hph+*	This study

Name	Description or sequence	Reference
Plasmids		
pMF272	*Pccg-1::sgfp+*	Freitag et al. 2004
pJV15-2	*Pccg-1::mchfp+*	Verdín et al. 2009
pMF334	*Pccg-1::drfpN+*	Freitag and Selker, 2005
pZero	Pccg-1::10Xgly::gfp+::loxp+::hph+::loxp+	Honda et al., 2009
pRR1-0mChFP	Pccg-1::10Xgly::*mchfp*+::loxp+::hph+::loxp+	This study
pRM01-RR01	*Pccg-1-tbg::sgfp+*	This study
pRM61-RR04	*Pccg-1-pcp-1::sgfp+*	This study
pRM91-RR13	*Pccg-1-drfp+::aps-2*	This study
pRM99-TR01	*Pccg-1-mzt-1::sgfp+*	This study
Oligonucleotides	**Sequence 5́-3́**	
GlyF	GGCGGAGGCGGCGGAGGCGGAGGCGGAG	Freitag lab
LoxpR	TGCTATACGAAGTTATGGATCCGAGCTCG	Freitag lab
FPPacF	TTAATTAACATGGTGAGCAAGGGCGAGGAG	This study
FPEcoR	CGAGCTCGGATCCATAACTTCGTATAGCA	This study
hphSMF	AAAAAGCCTGAACTCACCGCGACG	Riquelme et al, 2014
hphSMR	GGTCATTGACTGGAGCGAGGCGA	Riquelme et al, 2014
TBGF	CAATTCTAGAATGCCCAGAGAAATAATAAC	This study
TBGR	GCTATTAATTAAAGCCATTCTCTTGTCCG	This study
PCP-1xbaF	GCTCTAGAATGGTCCAGCCGGGCGTC	This study
PCP-1 pacR	CCTTAATTAAGATAGCAGCCCCCCTCA	This study
N-Aps1-SpeI-F	GGACTAGTATGGAGGAAGAAGCCC	This study
Aps-1-FseI-NG-R	ATGGCCGGCCCTAGGATCCCCTTTCG	This study
Tbg5'F	TTCTTTCCTACTCGAGCGACTGAA	This study
Tbg5'R	CCTCCGCCTCCGCCTCCGCCGCCTCCGCCA GCCATTCTCTTGTCCGT	This study
Tbg3'F	TGCTATACGAAGTTATGGATCCGAGCTCGG TCTTAGCCGGACAGATGAT	This study
Tbg3'R	TTTTCTTCCTGGGGAAGTTGGAGCAA	This study
PCP15'F	AAAAAGCTCGAGCGGGCGAGAA	This study
PCP13'R	CCTCCGCCTCCGCCTCCGCCGCCTCCGCCG ATAGCAGCCCCCCTCAT	This study
PCP13'F	TGCTATACGAAGTTATGGATCCGAGCTCGT CATGGTCATGACAACGTA	This study
PCP13'R	TTGAAAGTCAAAATACCGAGTCTTCTT	This study
rcSPA10_5F	ACAACGAGGATGAGTACGACAATGAG	This study
rcSPA10gly_5R	CGCCTCCGCCTCCGCCGCCTCCGCCATCCCTCAACAAGCTTCCAGTC	This study
rcSPA10loxp_3F	CGCCTCCGCCTCCGCCGCCTCCGCCATCCCTCAACAAGCTTCCAGTC	This study
rcSPA10_3R	GAAGAGGCAGAAAGTTGGCTGCGAC	This study
MztXbaIF	CTCTAGAATGGAGAAGAGCGAAAAACAGG	This study
MztPacIR	CTTAATTAATTTTCGGCGAGCTGCACTGG	This study

(*continued on next page*)

Table 2 (*continued*)

Name	Genotype	Reference
MZT1-5'F	AGGAGAGGAACCAGTTTAGG	This study
MZT1gly-5'R	CTCCGCCTCCGCCTCCGCCGCCTCCGCCTTTTCGGCGAGCTGCACTG G	This study
MZT1loxp-3'F	TGCTATACGAAGTTATGGATCCGAGCTCGATGATCGGCGGGGAGA GGGT	This study
MZT1-3'R	AGGAGATCTTCTAGAAAGATGCCAGATCTAACTGCTACTG	This study

incubated at 30°C until the cells reached a young mycelium stage (~16 h). An agar block was cut with the membrane and mycelia and was observed following the procedure described for laser scanning confocal microscopy. After a few min, we replaced the VMM agar block with a VMM- BML agar block (0.5 μg ml^{-1}) and immediately recorded the MTs depolymerization process. After 20 min, when MTs were completely depolymerized, we replaced the VMM-BML agar block with a VMM agar block. *De Novo* Mts nucleation was recorded until we observed a recovered microtubular cytoskeleton.

2.8. Phenotypic characterization of null mutant strains

To characterize the phenotype of mutant strains, we measure colony growth rate, hyphal growth rate, biomass production, branching rate, and conidiation rate. Colonial and hyphal morphology were compared with a WT strain; all measurements were done in triplicate. The *N. crassa* knock-out strains were obtained from the Fungal Genetics Stock Center (FGSC) (McCluskey, 2011) and corroborated using standard PCR techniques.

2.9. Growth rate

Conidia were inoculated (1 X 10^6 spores ml^{-1}) in 15 cm-VMM plates and incubated at 30°C for 48h. The colony growth rate was calculated in cm d^{-1}, measuring the colony radius every 6 h in ten different transects until the plate corresponding to the WT strain was filled. The growth rate was calculated with the elongation difference every 6 h, and data were stored and processed in Microsoft® Excel® for Microsoft 365 MSO (Version 2206).

2.10. Biomass production

The biomass production was determined in liquid cultures: 1 x 10^6 conidia ml^{-1} were inoculated in 100 ml of MMV and incubated at 30°C in constant agitation (150 rpm) for 72 h. The grown mycelium was collected by filtration on a Whatman filter paper No. 3 previously weighed. The Whatman paper containing the mycelium was dried and weighed, and biomass production was calculated in mg d^{-1}.

2.11. Branching rate

The WT and Δ*spa-10,* and Δ*spa-18* strains were inoculated in VMM plates and incubated at 30°C for 24 h, then observed with a stereomicroscope Olympus SZXILLB2-100 (Olympus, Tokyo, Japan) at 90x magnification. Images were captured with a CCD camera Olympus DP70 and analyzed with the software of the camera. The number of branches of leading hyphae was counted in the first 500 μm from the tip (branches/500 μm).

2.12. Conidiation rate

VMM plates were inoculated with WT or Δ*spa-10* and Δ*spa-18* strains and incubated at 30°C for 7d. Conidia were collected in 5 ml of a 1 M sorbitol solution, and the conidia were counted using a Neubauer chamber with an Olympus compound microscope.

2.13. Expression of MTB-3-GFP in the Δspa-10 and Δspa-18 strains

To express MTB-3-GFP in the Δ*spa-10* and Δ*spa-18* background, we cross the mutant strains with the XTL2-1 (*mtb-3-sgfp)*. Strains were crossed routinely on plates of synthetic crossing medium (SCM) supplemented with 1% sucrose and 2% agar (Davis, 2000), as previously described. Colonies were transferred to 1 ml culture tubes with VMM and incubated for 24 h at 30°C and screened to select for hygromycin resistance and GFP expression.

2.14. Live cell imaging with Laser scanning confocal microscopy

Strains were analyzed under two different confocal microscopes: An inverted Olympus Fluoview TM FV1000 confocal microscope (Tokyo, Japan) equipped with an argon laser (GFP: excitation, 488 nm; emission, 505-525 nm) and a diode pump solid-state (DPSS, Melles Griot, Carlsbad, CA) laser (mChFP or dRFP: excitation, 488 nm; emission, 560-660 nm) was used for individual or sequential visualization of GFP, mChFP or dRFP. A 60x Plan Apo N (Olympus) oil-immersion objective (NA, 1.42) was used. Confocal images were examined using FV10-ASW software (version 4.0.2.9, Olympus). To obtain the cellular dynamics of the FP-tagged proteins with a higher frame rate, an inverted confocal microscope Nikon ECLIPSE Ti-E Ti-E/B equipped with Spinning Disk CSU-200x1 Yokogawa and an argon-ion laser for excitation at 488 nm for GFP and an Apo 60X/1.49 N.A. oil immersion objective was used. Images were captured with an ANDOR iXon Ultra camera (Oxon, UK) and analyzed with NIS-Elements View 4.20 software.

2.15. Fluorescence recovery after photobleaching (FRAP) experiments

To determine Mt nucleation at the septal pore, we followed fluorescence recovery after photobleaching using an inverted Olympus Fluoview TM FV1000 confocal microscope (Tokyo, Japan). A selected region of interest in a septum was overexposed at 90% laser intensity for 4 s (argon laser 488 nm wavelength). Previously and after photobleaching, images were continuously scanned for up to 20 sec. FRAP experiments were repeated ten times.

2.16. Protein extraction, co-immunoprecipitation assays (Co-IP), and protein identification

To explore the protein-protein interaction in the MTOCs of *N. crassa*, we selected four strains: γ-tubulin-GFP (TRM01-RR01), MZT-sGFP (TRMXX-TR01), dRFP-APS-2 (TRM-128-RR10), and SPA-10-sGFP (TRM129-RR11). As controls, we also include a strain expressing cytosolic GFP (Cyt-sGFP) and a WT strain (FGSC4200). Before each experiment, all strains were activated on VMM agar, and the expression of the fluorescent protein was corroborated by Confocal Microscopy. Mycelia of the strains of interest were obtained by incubating conidia (1 X 10^6 spores) in liquid VMM at 30°C, 150 rpm for 3 d (in the dark). The mycelia were frozen in liquid nitrogen and ground, continuously adding liquid nitrogen until having a fine powder. One g of biomass was suspended in 1 ml ice-cold extraction buffer (100 mM Tris-HCl pH 7.5, 100 mM NaCl, 0.5 mM EDTA, 2.5 mM, and 1 mM PMSF, and Protease Inhibitor Cocktail (AEBSF 100 mM, E-64 1.4 mM, Pepstatin A 2.2 mM 1,10-Phenanthroline 500 mM; Sigma-Aldrich-Cat. P8215-1ML). Insoluble material was discarded by centrifugation at 4°C, at 12,000 rpm for 10 min. Supernatants were clarified through a 0.22 μm syringe filter.

The total protein amount was quantified by the Bradford method, and the integrity and fluorescence of the proteins were verified on 10% native PAGE. The Co-IP was carried out with GFP-Magnetic agarose pearls (GFP-Trap®_M Cromotek) to capture the sGFP and dRFP-labeled proteins and their physical interactors (in native states). The agarose pearls were previously washed and equilibrated in extraction buffer. Then, 1 ml of native extracts (4-6 mg ml^{-1}) was incubated with 10-15 µl of beads overnight at 4°C, under constant mixing in a tube roller. The magnetic pearls were pull-down in a magnetic rack and washed six times with 500 µl ice-cold extraction buffer. The pearls were resuspended in 50 µl 2x SDS-Sample buffer (65.8 mM Tris-HCl, pH 6.8, 2.1% SDS, 26.3% glycerol, 10% 2-mercaptoethanol, 0.01% bromophenol blue), boiled for 5 min at 95°C and centrifuged at 12,000 rpm for 1 min. Eluted proteins were separated in 8% SDS-PAGE gels and stained with Coomassie blue. Two replicates per experiment were sent for protein identification service. The gel lanes were aseptically cut with a scalpel and stored in a 15 ml tube with distilled sterile water at 4°C (2 lanes per tube). The samples were sent to Creative Proteomics for nano Liquid Chromatography with Tandem Mass Spectrometry LC-MS/MS. Protein annotation was based on the FungiDB Fungal and Oomycete Genomics Resources database (https://fungidb.org/fungidb/) *Neurospora crassa* database. According to the algorithms (on multiple leves) used by Creative Proteomics Inc. the threshold for significative associations was a score > 50 for high-confident results. The selected proteins were also present in other analyses that we made (STRING, Panther and Kegg). Nevertheless, the interactors network was based on the prediction of String, the results of Co-IP, considering only those with a higher score and intensity than the controls (GFP-Cyt and WT).

3. Results

3.1. MTs are nucleated from SPBs and foci in the cytoplasm.

To determine locations of MT origin, we aimed to visualize putative MTOCs in *N. crassa.* To this end, orthologs for all known centrosomal and non-centrosomal MTOC components were identified in the genome of *N. crassa* (Table 1). We identified γ-tubulin (NCU03954) with 454 aa with an identity of 76.6% with Gtb1 of *S. pombe* and 82.7% with MipA of *A. nidulans*. For the γ-tubulin complex (γ-TuRC) targeting proteins, we identified PCP-1 (NCU0241) of 1, 207 aa with 27.7% identity with Pcp1 and 32.3% and with PcpA of *S. pombe* and *A. nidulans* respectively; APS-2 (NCU17239) of 1,115 aa with 23.7% identity with Mto1 in *S. pombe* and 43.3% with ApsB of *A. nidulans*, and a small protein named MZT-1 (KHE87685.1) with only 80 aa sharing 44% identity with Mzt1 from *S. pombe* and 57.6% identity with MztA from *A. nidulans* (Supplementary Figures S1 and S2).

A heterokaryon strain expressing β-tubulin-GFP and γ-tubulin-mChFP was used to observe MT repolymerization after the exposure to the anti-MT drug benomyl. The strain was grown on VMM-agar onto a cellophane membrane that was cut and observed by confocal microscopy previous to the exposure to benomyl, using the inverted agar block method (Hickey et al., 2002). After 5 min (Figure 1Aa), the VMM-agar block was removed and replaced with a VMM-BML-agar block (benomyl 0.5 µg ml^{-1}), and a timelapse movie was recorded to observe MT depolymerization. To describe the events related to MTOCs in *N. crassa* hyphae, we defined three hyphal regions: region I containing the Spitzenkörper, region II extending from the posterior side of the Spitzenkörper through the anterior side of the first nucleus, and region III extending over a variable distance from the anterior side of the first nucleus towards a zone characterized by the presence of large vacuoles (Ramos-Garcia et al., 2009). After 5 min of exposure, MTs started to depolymerize and completely disappeared after 15 min (Fig. 1Ab). Just some β-tubulin-GFP fluorescent puncta were left in the cytoplasm, and γ-tubulin-mChFP remained associated with nuclei. To induce MT recovery, we replaced the VMM-BML-agar with a VMM-agar block. In the following 2 min of incubation, short MTs appeared, some associated with γ-tubulin-mChFP from the SPBs and some in the cytoplasm of the region I and II independent of γ-tubulin. Only few MTs repolymerized around the Spk area (region I) (Figure 1Ac, Supplementary Movie S1). After ~4 min, MTs were longer (Figure 1Ad), and after 15 min, the microtubular cytoskeleton was recovered (Figure 1Ae). The number of MTs nucleation events in the cytoplasm in the region I and II (9.9±1.9 MTs n=7) was very similar to the MTs nucleation associated with nuclei (region III) (9.4±1 MTs n=7) ($P>0.05$) (Figure 1B).

Using FRAP, we analyzed putative MT nucleation at the septal pore (Figure 1Ca-1Cd). Before treatment, MT-bundles were gently pressed in the septal pore. Same as in regions I and II during BML exposure, after ~5 min MTs were depolymerized, and after 14 min of removing benomyl, we observed MTs going through the septal pore (Figure 1Cd). However, MTs did not repolymerize from the septum. Most of the MTs came from the adjacent regions, following the cytoplasmic bulk flow. MTs passed through the septal pore, and some seemed transiently anchored. We repeated the experiment using a strain expressing MTB-3-mChFP and β-tubulin-GFP with similar results (data not shown). We did observe MTB-3-mChFP at the septal pore.

3.2. Localization of N. crassa MTOCs components in living cells

We analyzed the dynamics and localization of proteins associated with MTOCs, such as γ-tubulin, APS-2, PCP-1, and MZT-1, labeled either with GFP, dRFP or mChFP by confocal microscopy. All proteins were distributed along the cytoplasm as bright fluorescent spots associated with nuclei in conidia, germlings (Supplementary Figure S3), and mature hyphae (Figures 2A and 3A). γ-tubulin-mChFP, PCP-1-mChFP (Figure 2A), and MZT-1-GFP (Figure 3A) were distributed along region III but absent in the nuclear exclusion zone (region I and II) except dRFP-APS-2 (Figure 2A) that was free in the cytoplasm in those regions.

To confirm the localization of γ-tubulin-GFP and MZT-1-GFP in the nucleus, we independently co-expressed these two proteins with H1-dRFP. Both proteins were associated with nuclei and the SPBs (Figures 2C and 3A). We also co-expressed PCP-1-mChFP and dRFP-APS-2 with the nucleoporin protein SON-1-GFP to show their relation with the nuclear envelope (Figure 2C). PCP-1-mChFP and dRFP-APS-2 were organized in layers embedded in the nuclear membrane. Furthermore, PCP-1-mChFP was localized at the SPB inner plaque in the nucleoplasm and dRFP-APS-2 at the outer plaque of the SPB (Figure 2C). To confirm the association of γ-tubulin with the γ-TuRC targeting proteins PCP-1 and APS-2, we analyzed two heterokaryons co-expressing γ-tubulin-GFP with PCP-1-mChFP and dRFP-APS-2 respectively. Confocal images showed partial co-localization of γ-tubulin with PCP-1 and APS-2 (Figure 2D and 2E). Supporting the idea that, as in other organisms, γ-tubulin might be recruited by PCP-1 to the inner plaque of the SPB and by APS-2 to the outer plaque in *N. crassa.*

The association between MZT-1, γ-tubulin, PCP-1, and APS-2 was also analyzed by confocal microscopy. MZT-1-mChFP and γ-tubulin-GFP co-localized almost entirely at the SPB (Figure 3B). Both proteins were duplicated and positioned at opposite sites of the nucleus during mitosis, although during interphase, only one bright spot was observed at one nuclear pole (Figure 3). MZT-1 also co-localized with PCP-1 and APS-2. In the heterokaryon expressing MZT-1-mChFP and PCP-1-GFP, we found that the MZT-1-mChFP protein overlapped with the PCP-1-GFP fluorescent signal, but the PCP-1-GFP spot looked bigger (100% overlapping; n=50) (Figure 3C). However, the association between MZT-1-GFP and dRFP-APS-2 was only partial (86% overlapping; n=50) (Figure 3C). The co-localization of PCP-1- GFP and dRFP-APS-2 showed a lower correlation (84% overlapping; n=50) (Figure 3C). This suggests that MZT-1 is localized between the inner and the outer plaque of the SPB.

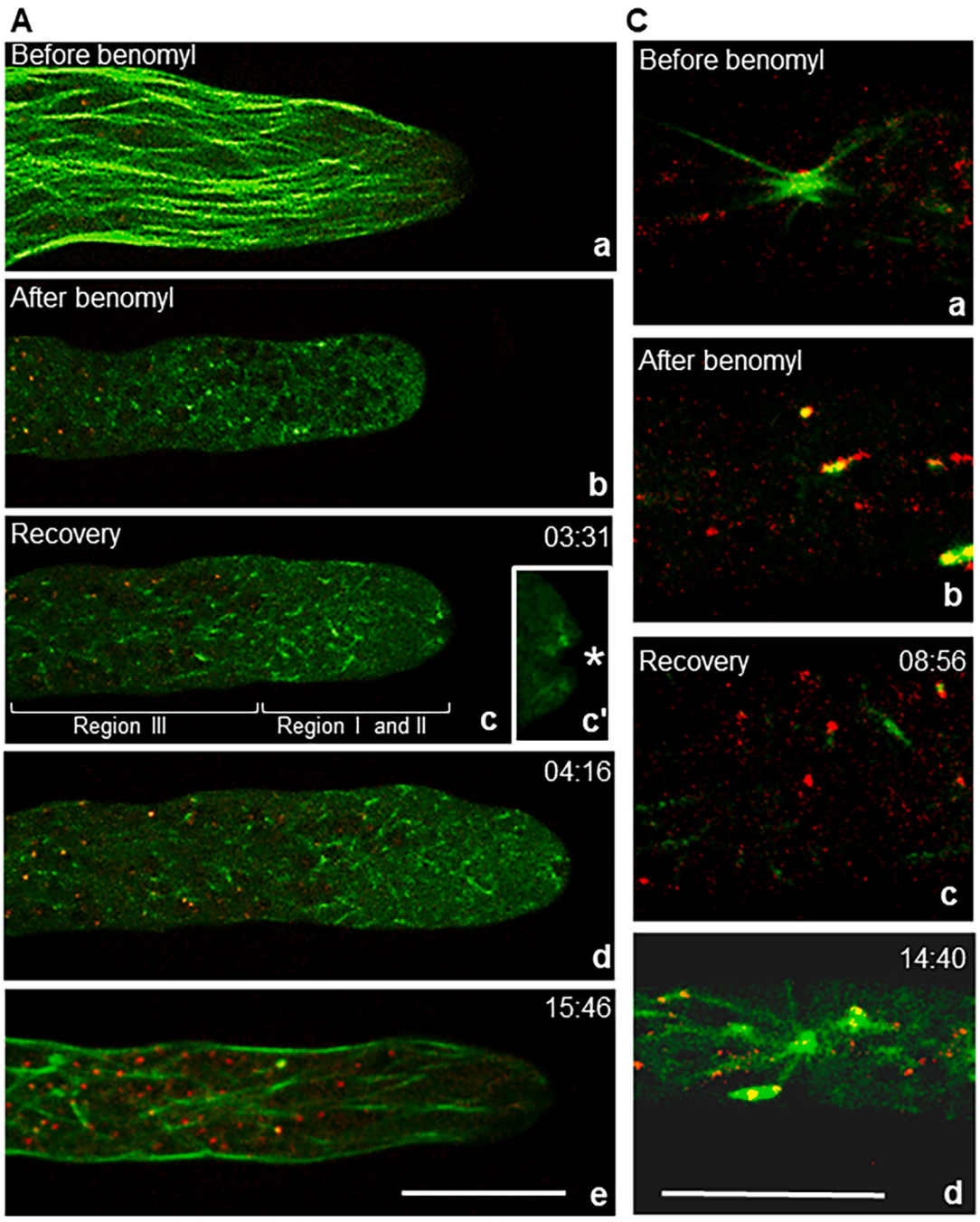

B

MTs nucleation events	Regions I and II	Region III
	9.9 ± 1.9	9.4 ± 1.0
	Cytoplasmic	SPB associated

Fig. 1. Microtubule nucleation after benomyl treatment. (A) Apical and subapical region of *N. crassa* hypha expressing β-tubulin-GFP and γ-tubulin-mChFP. (a) Hypha before treatment with benomyl. (b) Hypha after treatment with 0.5 mg ml^{-1} benomyl. MTs were totally depolymerized, just bright puncta were left distributed along the hypha. (c) 03:31 min after benomyl removal, MTs repolymerized associated with γ-tubulin-mChFP in Region III and also γ -tubulin-independent in Region II, some of them were organized close to the Spk (Asterix) area (c'). 04:16 min after benomyl removal, MTs increased their number and length. (e) MTs completely recovered after 15 min. (B) Number of MTs repolymerized in region I and II compared with region III. There was no difference in the number of repolymerization events associated with and not associated with γ -tubulin. (C) Mature septum of *N. crassa* hypha expressing β -tubulin-GFP and γ -tubulin-mChFP. (a) MTs were bundled in the septal pore before the treatment with benomyl. (b) Septum after complete MT depolymerization after benomyl treatment (c and d) Two time points after removing benomyl. MTs did not polymerize from the septum, the recovery of fluorescent MTs was produced by their transport through cytoplasmic bulk flow. Time in minutes: seconds. Scale bar=10 μm.

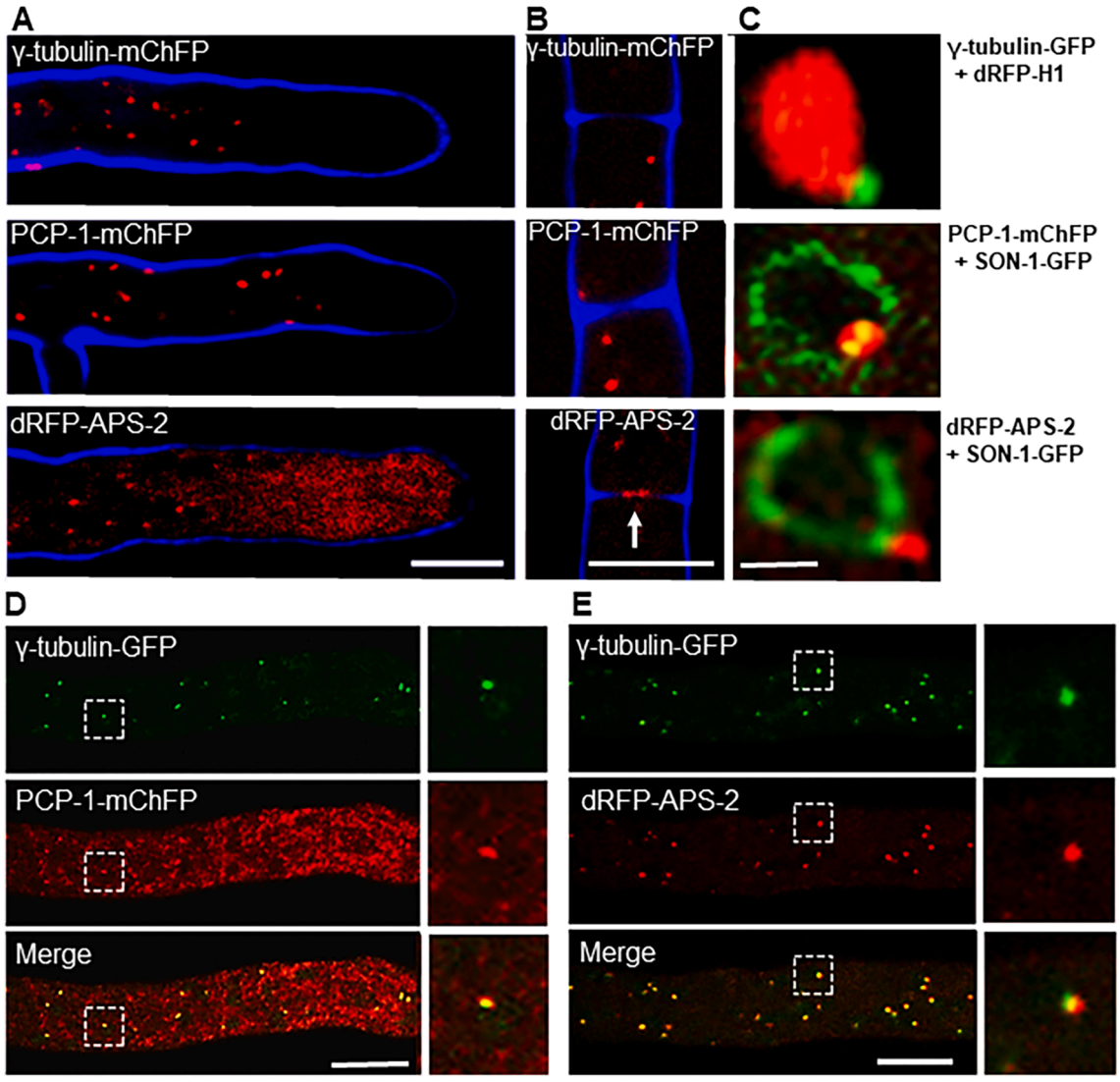

Fig. 2. Localization of γ -tubulin, PCP-1, and APS-2 in *N. crassa*. (A) γ-tubulin-mChFP, PCP-1-mChFP, and dRFP-APS-2 were accumulated as small bright spots associated with SPBs. APS-2 was also present in the cytoplasm in Region I. (B) γ -Tubulin-mChFP and PCP-1-mChFP were not present at septa, but dRFP-APS-2 was associated with the septal pore. Cell wall labeled with calcofluor white. (C)) γ -tubulin-GFP was associated with the SPB (nucleus labeled with dRFP-H1), PCP-1-mChFP was embedded in the inner plaque and dRFP-APS-2 was in the outer plaque of the nuclear envelope labeled with the nucleoporin protein SON-1-GFP. (D) Co-localization of γ-tubulin-GFP and PCP-1-mChFP in the SPB. (E) Co-localization of γ-tubulin-GFP and dRFP-APS-2 in the SPB. Scale bar=10 μm.

3.3. Microtubule organization at the hyphal tip and septal pore is independent of γ-tubulin

To describe the association of the MTs with γ-tubulin, PCP-1, APS-2, and MZT-1, we co-expressed individually the MTOC components tagged with fluorescent proteins with strains expressing either β-tubulin-GFP or -mChFP. As previously shown (Mouriño-Pérez et al., 2006), MTs were extended throughout the cytoplasm, mainly arranged longitudinally along the hyphae. Most MTs showed some curvature with a long pitch and a tendency to intermingle, forming a loosely braided network throughout the cytoplasm (Figure 4). γ-Tubulin, PCP-1, APS-2, and MZT-1 were localized at one pole of the nuclei-associated MTs (Figure 4). We observed mitotic nuclei with duplicated SPBs and MTs associated with these structures (Figure 4B and 4C). MT bundles were packed at the septal pore, and APS-2 was also present on the edge of the septal pore, but neither γ-tubulin nor PCP-1 or MZT-1 were detected in that region (Figure 2B, 3D).

3.4. APS-2 is an MTOC component present in septa

APS-2 was associated with SPBs (Figure 2A, 2C, and Supplementary Figure S3C) and accumulated at the septal pore (Figure 2B and Supplementary Figure S3C). Surprisingly, none of the other components of the MTOCs, such as γ-tubulin, PCP-1, and MZT-1, were present at septa (Figure 2B and 3D).

To determine the time of recruitment of APS-2 during septum formation, we constructed a kymographic time-series of the septal constriction in mature hypha expressing dRFP-APS-2 and the cell wall stained with calcofluor white. We found that APS-2 is a late recruited protein that arrived at the septation site ~7 min after plasma membrane ingrowth when the septum was fully formed and reached the maximum accumulation after 12 min (Figure 5A, Supplementary Movie S2). Figure 5B shows a 3D reconstruction of the septal pore after dRFP-APS-2 was recruited. It was distributed in a disk-like shape, surrounding the septal pore (Figure 5B, Supplementary Movie S3). We used a strain expressing fimbrin tagged with GFP (Fim-GFP), an actin-binding protein associated with the septation process (Delgado-Alvarez et al., 2010), fused it to a strain expressing dRFP-APS-2 to observe their temporal

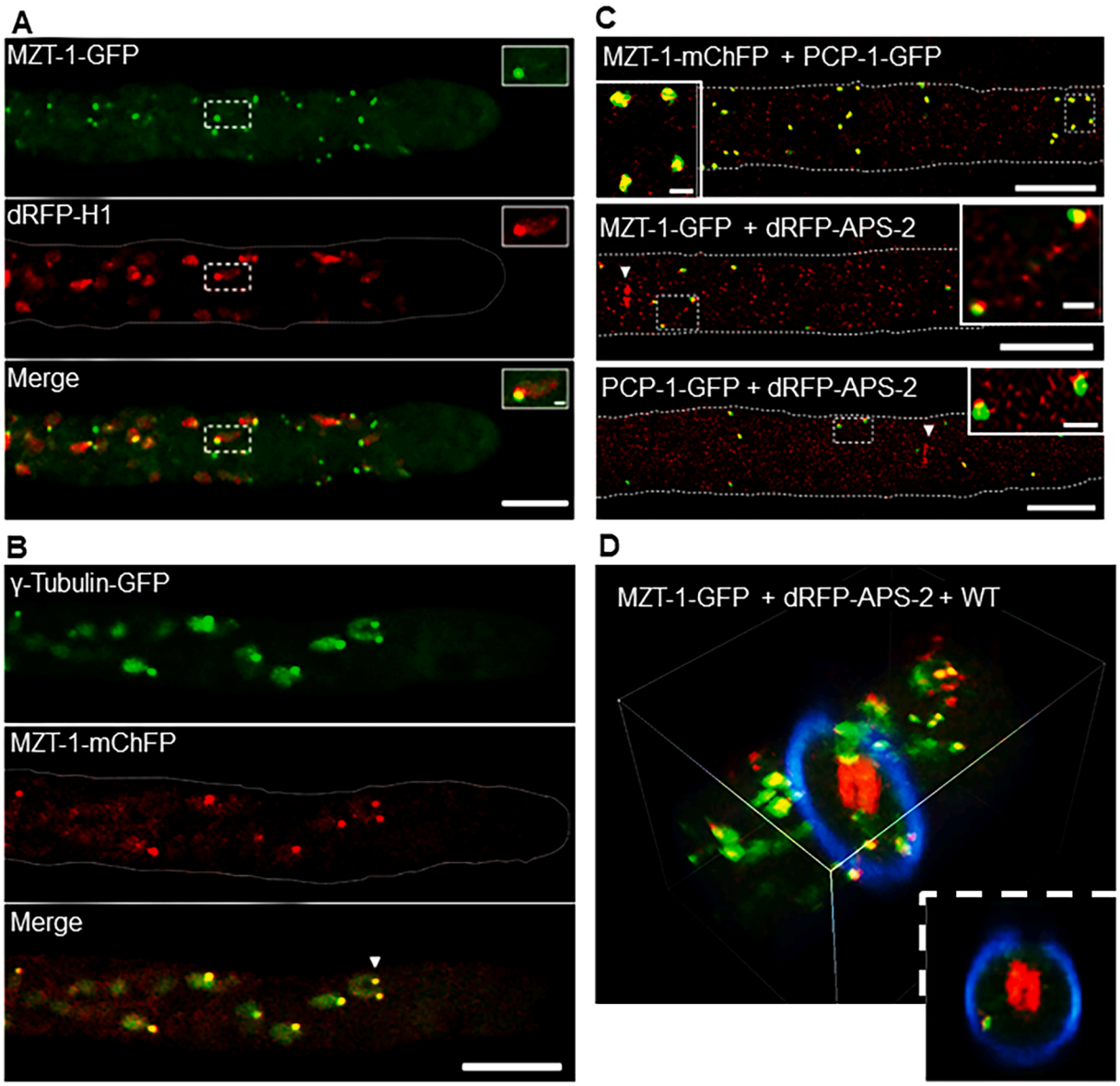

Fig. 3. Localization of MTZ-1-GFP in *N. crassa*. (A) MTZ-1-GFP formed small bright spots associated with nuclei labeled with dRFP-H1 (B) co-localization of MTZ-1-mChFP with γ -tubulin-GFP, dRFP-APS-2, and PCP-1-GFP in the SPB. Arrowhead points to nuclei in mitosis (C) Association of MTZ-1-mChFP with PCP-1-GFP, and with dRFP-APS-2 and association of PCP-1-GFPwith dRFP-APS-2, all these proteins are organized in layers shown by the partial co-localization. (D) Co-localization of MZT-1-GFP and dRFP-APS2 at a septum. Cell wall stained with calcofluor white. There was no localization of MZT-1 in septa. Scale bar=10 μm.

association. The appearance of dRFP-APS-2 surrounding the septal pore after Fim-GFP was no longer associated with the septum (Figure 5C). These findings showed that APS-2 was not associated with the septation process and was recruited to mature septa.

3.5. The outer plaque and septal pore protein APS-2 appears to be an essential protein

The deletion of *tbg*, *pcp-1* and *aps-2* led to homokarytic lethality. We characterized the features of the *aps-2* gene mutant in a heterokaryotic state (Δ*aps-2*^{HET}). The Δ*aps-2*^{HET} mutant was steril as both donor and acceptor (Figure 6A), and it had a significant defect in the elongation rate (Figure 6B). Hyphae also appeared different from WT and displayed a meandering phenotype. The Spk size or position were not affected (Figure 6C). Only the Δ*mtz*-1 mutant was viable. The homokaryon Δ*mzt-1* knock-out null mutant was viable, but it had a strong phenotype (Figure 6E-D). Growth, branching, and conidiation were severely reduced (Figure 6D-6I). It was not surprising that *tbg* and *pcp-1* were essential, considering their important functions in mitosis. However, a vital role was not expected for APS-2.

3.6. SPA10 is a component of septa and is associated with the MT plus-end protein MTB-3

The septal pore-associated proteins SPA10 and SPA18 were described in *N. crassa* as disordered proteins that aggregate at septa (Lai et al., 2012). In *A. nidulans,* homologs of Spa10 and Spa18 are key elements of sMTOCs, where Spa10 targets the Spa18/ApsB complex to anchor the sMTOCs to the septal pore (Gao et al., 2019; Shen et al., 2014; Zhang et al., 2017a). We found dRFP-APS-2 in N. crassa septa, so we examined a strain expressing SPA10 tagged with GFP. SPA10-GFP was accumulated close to the edge of the septal pore (data not shown). The association of APS-2 and SPA-10 was analyzed by Co-IP experiments described below.

In previous studies of our group about the homolog of EB1, an MT plus-end associated protein named MTB-3 in *N. crassa*, we found an

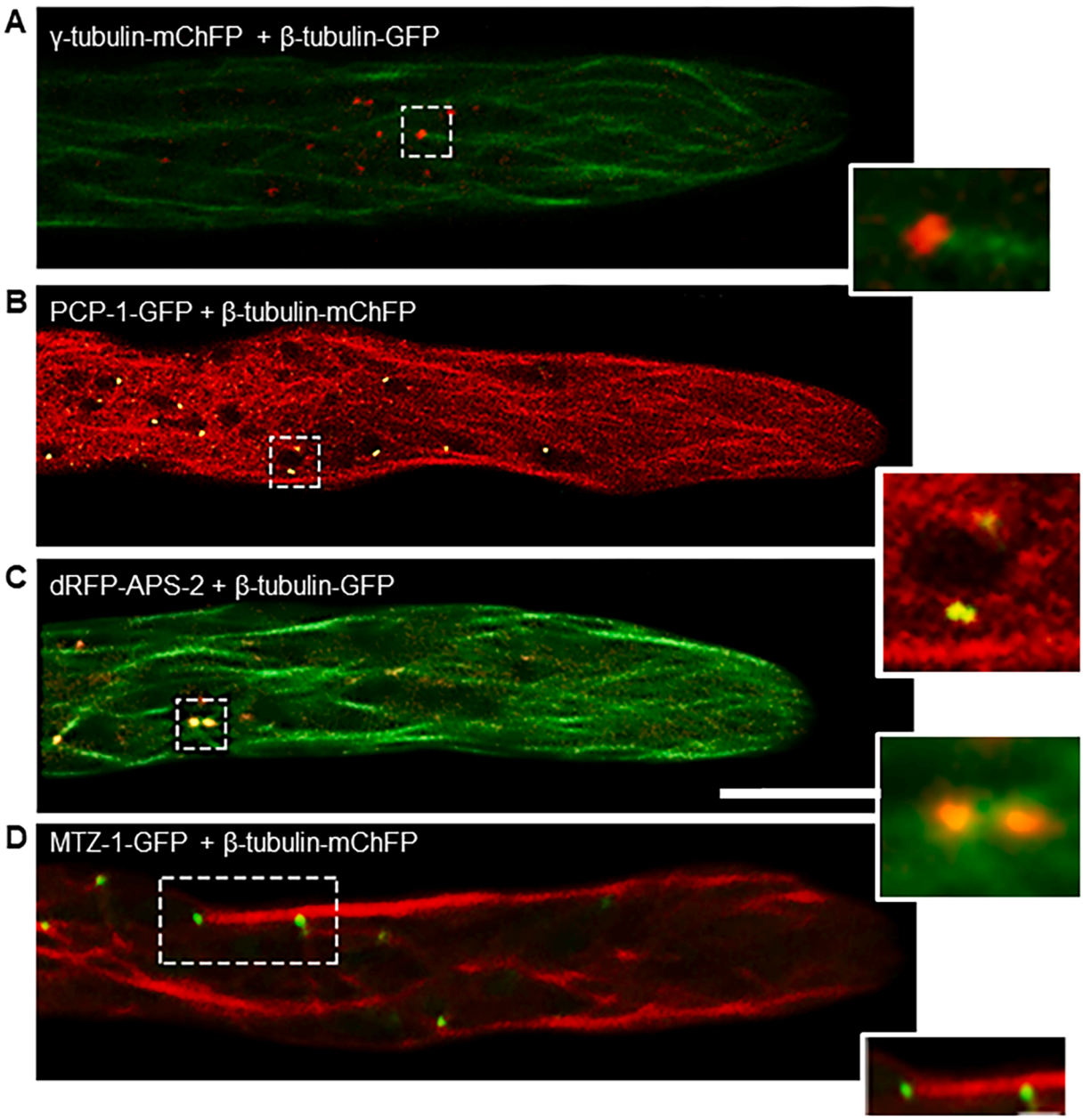

Fig. 4. Association of MTOC proteins with MTs. Each panel shows the zoom-in of a detail of the interaction of MTs with each protein (A) Co-expression of γ-tubulin-mChFP and β-tubulin-GFP. (B) Co-expression of PCP-1-GFP and β-tubulin-mChFP. (C) Co-expression of dRFP-APS-2 and β-tubulin-GFP. (D) Co-expression of MTZ-1-GFP and β-tubulin-mChFP. Scale bar=10 μm.

accumulation of this protein surrounding the septal pore (Mouriño-Pérez et al., 2013). Therefore, we explored whether SPA10 could be associated with MTB-3. We produced a strain expressing MTB-3-mChFP and SPA10-GFP. As shown before, MTB-3-mChFP was distributed as fast-moving comets decorating the MTs plus-end, and additionally, it was accumulated at the septal pore, partially co-localizing with SPA10-GFP (Figure 7A). The 3D reconstruction of confocal Z-stacks showed MTB-3-mChFP accumulated in the center of the septal pore, and some comets seemed to be associated with this accumulation. The MTB-3-mChFP signal was embedded in a spot corresponding to SPA10-GFP (Figure 7A and 7B). Next, we performed a FRAP experiment to observe the turnover of these two proteins at septa. MTB-3-mChFP was highly dynamic and recovered 19 sec after photobleaching, while few molecules of SPA10-GFP repopulated the septal region in 40 sec (Figure 7C).

3.7. SPA10 and SPA-18 are indispensable for MTB-3 activity at the septal pore

To get insights into the mechanism of how MTB-3 accumulates in the septal pore, we expressed MTB-3-GFP in Δ*spa-10* and Δ*spa-18* null mutants. MTB-3-GFP localization at septa was not affected either by the deletion of *spa-10* or *spa-18* (Figure 8). Nevertheless, we evaluated the FRAP of MTB-3-GFP in septa of a WT strain and in the Δ*spa-10* and Δ*spa-18* null mutants. We observed in WT a weak signal of MTB-3-GFP at the septal pore 6 sec after photobleaching and the fluorescence intensity gradually increased (Figure 8A). In comparison, the repopulation of the septal pore by MTB-3-GFP in the Δ*spa-10* and Δ*spa-18* mutants took between 10 - 12 sec (Figure 8B and 8C).

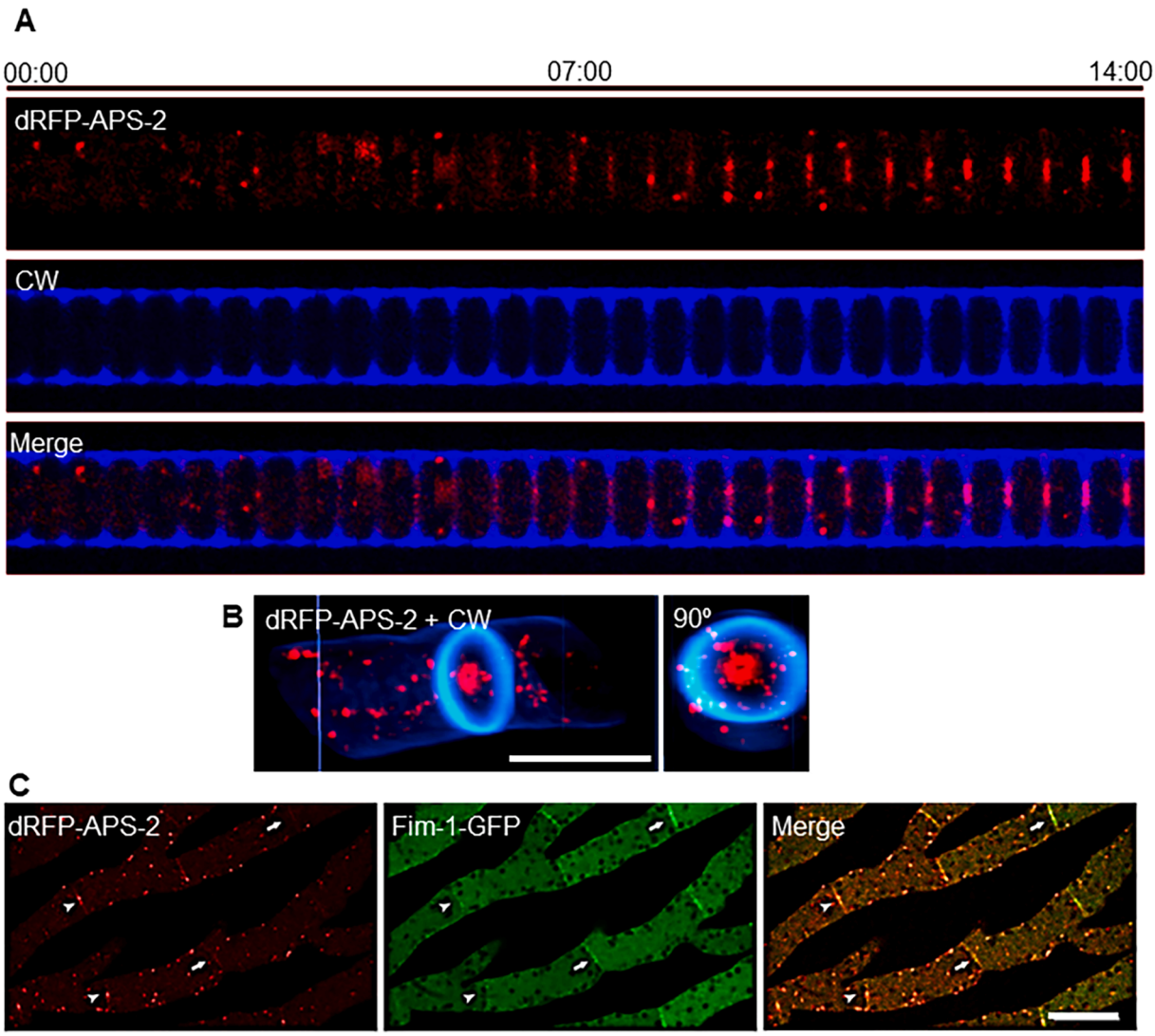

Fig. 5. APS-2 localized at mature septa. (A) Kymograph of the recruitment of dRFP-APS-2 during septum development (30 s interval). Time 0:00 points the beginning of cell wall ingrowth. At min 07:00, dRFP-APS-2 started to accumulate at the septal pore. The cell wall was stained with calcofluor white (CW). (B) 3D reconstruction of a confocal Z-stack, lateral and 90°clock-wise views. dRFP-APS-2 was distributed in a disk-like pattern surrounding the septal pore. Co-expression of dRFP-APS-2 with the actin-binding protein Fim-1-GFP. Fimbrin arrives at the septation process when the contractile actomyosin ring is formed. White arrows show early septation events where only fimbrin is transiently present in the septa and the white arrowhead indicates septa after fimbrin was not present anymore but dRFP-APS-2 was present. Scale bar=10 μm.

3.8. Molecular association among MTOCs components

Using the strains expressing γ-tubulin-GFP, MZT-1-GFP, dRFP-APS-2, and SPA10-GFP, we performed immunoprecipitation (Co-IP) assays using GFP-Trap and nano LC-MS/MS to analyze the set of proteins associated with each one. As a control, we also did the IP assay in a strain expressing cytoplasmic GFP (Cyt-GFP) and a WT strain. More than one thousand proteins were identified in each experiment using the *N. crassa* database (γ-tubulin-sGFP 1,788, APS-2-dRFP 1,722, MZT-1-sGFP 1,598, and SPA10-sGFP 1,638, WT 1,012 and Cyt-GFP 1,210). To narrow the findings, we targeted our analysis on the known MTOC components described in the literature, the septal-associated proteins (Lai et al., 2012), and septal proteins annotated in the UNIPROT database (81 proteins total). Table 3 shows the total number and the number of shared identified proteins in the four assays, and Table 3 presents the proteins associated with each target. γ-tubulin showed potential MTOC interactors APS-2, GCP-2, GCP-3, GCP-4, GCP-5, GCP-6, and proteins such as α and β-tubulin, CMD (Calmodulin), EB-1, Kinesin-13, Dynein, FACT (Facilitates Chromatin Transcription), and APS-1. In the Co-IP experiment, APS-2 and the members of the γ-TuSC, GCP-2, and GCP-3 were identified. Additionally, MZT-1-GFP was associated with α and β-tubulin, CMD, EB-1, Kinesin-13, Dynein, FACT, and Developmentally regulated GTP-binding protein 1-GTP-bd.

APS-2-GFP was associated with α and β-tubulin, CMD, EB-1, Kinesin-13, Dynein, FACT, and STU-11, the MT Polymerase. It had the highest score in the association with MTB-3. The intrinsically disordered septal protein SPA-10-GFP had a similar association to APS-2 except for dynein and STU-10. Nevertheless, neither of these two proteins was isolated in the corresponding experiments. Interestingly, neither PCP-1 nor SPA-18 were detected in any experiment.

3.9. Model for the Neurospora crassa MTOCs

A protein interaction network was built in STRING v.11.5 and modeled with Cytoscape v3.8.2 using MipA (AN0676.2), ApsB (AN3437.2), Mzt1 (AN1361), and SPA-10 (AN1948.2) of *A. nidulans* as inputs. Based on the predicted interactions, Co-IP results, and protein co-localization observed by confocal microscopy, we cured the information

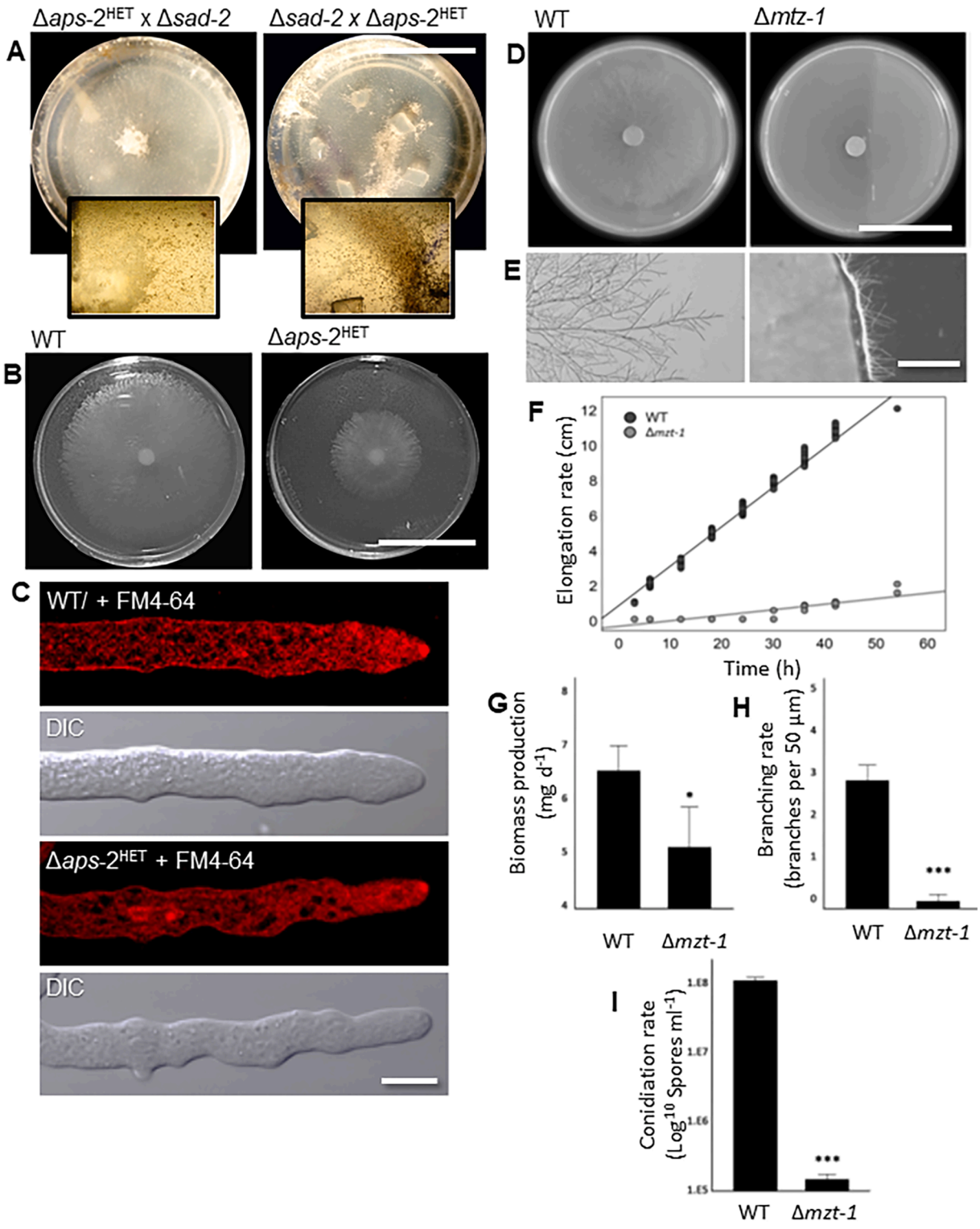

Fig. 6. Viable mutants of MTOC components. (A) Crosses of Δ*aps-2*^{HET} with Δ*sad-2* as a donor and as a receptor. There is no perithecia production. (B) Macroscopic morphology of the colony of Δ*aps-2*^{HET} mutant in its heterokaryotic stage. Elongation rate is visibly affected. (C) Hyphal morphology in the Δ*aps-2*^{HET} mutant compared with the WT. (D) Macroscopic morphology of the colony of the homokaryon Δ*mtz-1* mutant compared with the WT strain after 24 h of incubation. The mutant is viable but is strongly affected. (E) Images of the margin of the colony of the Δ*mtz-1* mutant showing small and thin hyphae. (F) Graph of the comparison of the elongation rate of Δ*mtz-1* mutant with the WT strain. Elongation was severely affected in the mutant. (G) Biomass production (H) Branching rate and (I) Conidiation rate were also harshly affected in the Δ*mtz-1* mutant. Scale bar=10 µm in (C) and 100 µm in (E).

and constructed an MTOC network for *N.* crassa (Figure 9A). The SPB components were grouped, most of which are directly related to γ-tubulin. Septal proteins did not interact with the core MTOC components, but they are linked to MTs by MTB-3. The interaction of SPA18 with SPA10, APS-2, or any MTOC components was not confirmed. However, we cannot discard SPA18 as an MTOC component similar to APS-2, but further testing has to be done. PCP-1 seemed to serve as a receptor of γ-TuRC at the SPB inner plaque, with MZT-1 associated

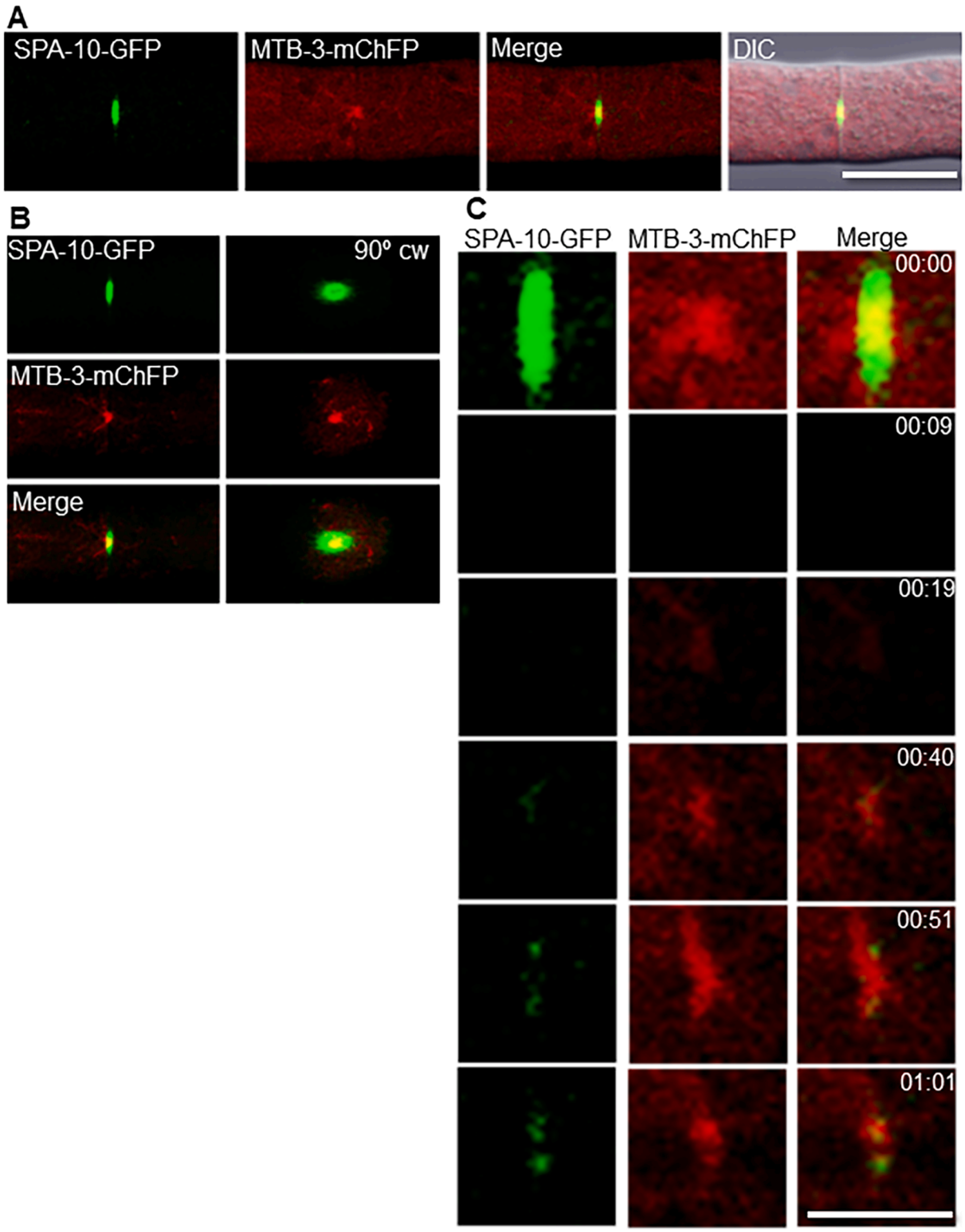

Fig. 7. Association between MTB-3-mChFP and SPA-10-GFP at the septal pore. (A) Co-expression of MTB-3-mChFP and SPA-10-GFP in a mature septum. (B) 3D reconstruction of confocal z-stack of MTB-3-mChFP and SPA-10-sGFP at the septal pore. Lateral and 90° Clock-Wise view. Scale bar=5 μm. (C) Time-lapse of fluorescence recovery after photobleaching of a septal pore. The first row of panels shows the septum before photobleaching. As SPA-10-GFP is a resident of the septum, there is almost no addition of new fluorescent molecules. However, MTB-3-mChFPis highly dynamic and repopulated the septal pore very fast. Time in min=sec. Scale bar=10 μm.

directly with the γ-TuSC (Figure 9). In contrast, APS-2 is localized at the outer plaque of the SPB and in septal pores interacting with SPA-10 (Figure 9). Thus, given the lack of core MTOC components at septa and Spk, we propose that γ-tubulin-dependent MTOCs in *N. crassa* are just present in the SPBs, and septa are receptors for MT plus ends where the MT network re-organizes and extends into the next compartment (Figure 9).

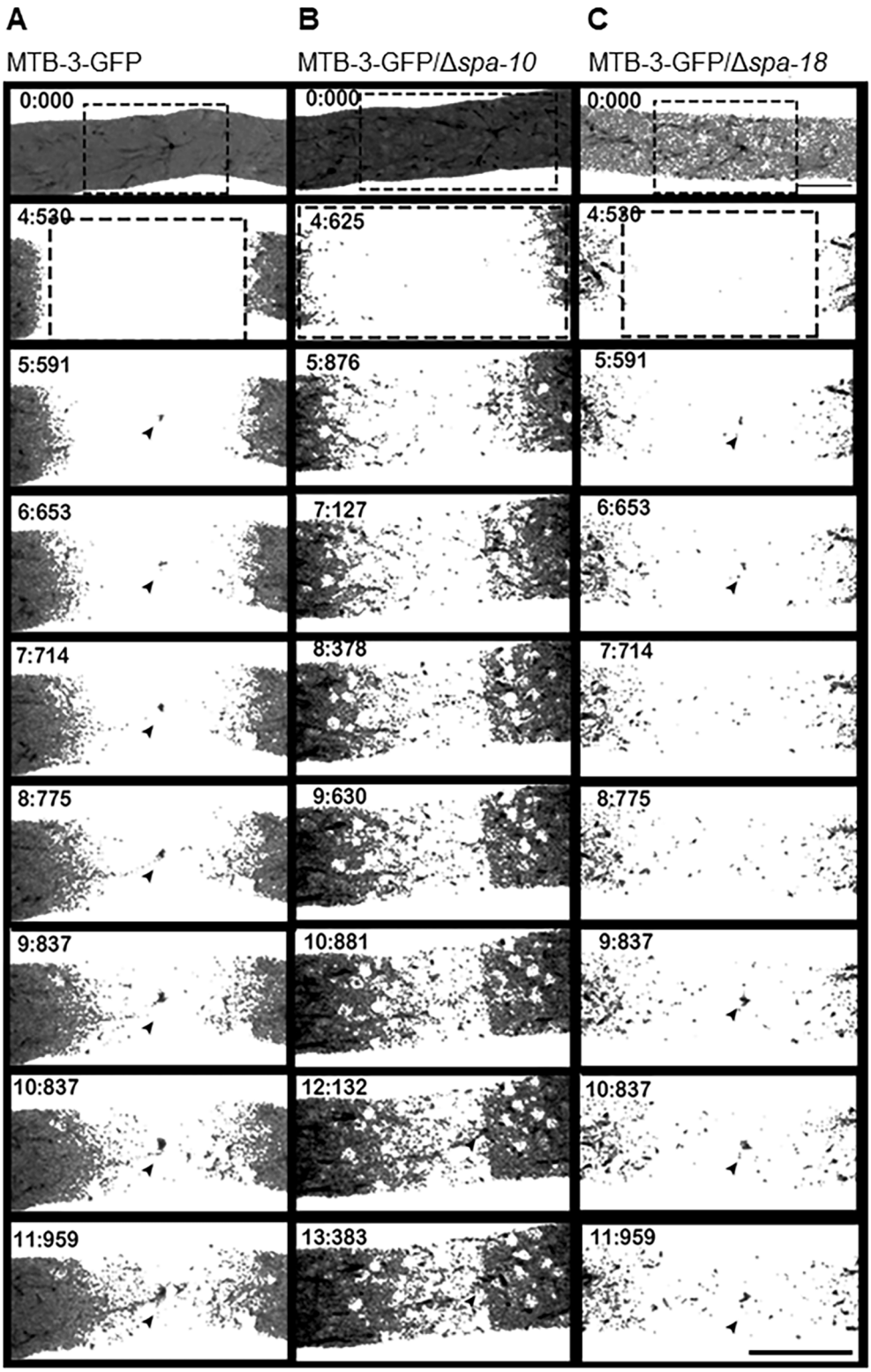

Fig. 8. Fluorescence recovery after photobleaching of MTB-3-GFP at the septal pore in a Δ*spa-10* and Δ*spa-18* deletion strain. Time-lapse of the fluorescence recovery of MTB-3-GFP at the septal pore in an (A) WT strain, (B) Δ*spa-10* mutant, and (C) Δ*spa-18* mutant. Rectangles with the discontinued line show the area photobleached. Arrowheads show the arrival of MTB-3-GFP to the septal pore. Time=seconds: milliseconds. Scale bar=10 μm.

4. Discussion

4.1. N. crassa, a fungus with ~100 MTOCs per compartment

The MT cytoskeleton is essential for the fast and continuous growth of filamentous fungi; therefore, the formation and functionality are very important. The fungal SPBs are the main MT organizing centers in *S. cerevisiae* and other fungi. However, like in vertebrates, the picture for fungi had to be extended because additional MTOCs were discovered in *S. pombe* and *A. nidulans*. In *N. crassa,* SPBs appear to be the main MTOCs

Table 3
Proteins isolated by Co-IP and identified by nano-LC MS/MS.

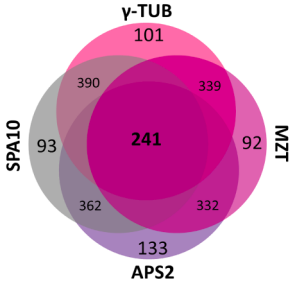

	CODE	Protein-Predicted functional partner	Controls		Experiments			
			WT	CYT	γ-TUB	MZT	APS2	SPA10
γ-TuSC	**γ-Tubulin**	***Tubulin gamma chain***		6.93	9.78	7.30		
	GCP-2	*Spindle pole body component*			9.20	7.15		
	GCP-3	*Gamma-tubulin complex protein 3*			9.53	7.34		
	GCP-4	*Gamma-tubulin complex protein 4*			8.76			
	GCP-5	*Gamma-tubulin complex protein 5*			8.51			
	GCP-6	*Gamma-tubulin complex protein 6*			8.84			
Other MTOC components	**MZT-1**	***Mitotic-spindle organizing protein 1***				8.79		
	APS2	***Anucleate primary sterigmata protein B***			6.78	6.52	7.97	
	ALP-1	*Dis1/XMAP215 protein AlpA*						
	PCP-1	*PACT_coil_coil domain-containing protein*						
	SPA18	*Septal pore-associated protein 18*						
	CMD-1	*Calmodulin A*	6.93	7.83	8.95	8.11	8.58	8.61
	CDC-11	*Centriolin*						
	SFI-1	*Sfi1-domain-containing protein*						
	CDC-31	*Centrin 3*						
	NDC-1	*Uncharacterized protein*						
Microtubules and relevant associated proteins	Act141	*Activator 1 41 kDa subunit*	7.09	7.85	7.63			
	An-Mlp1	*Nuclear pore complex protein An-Mlp1*	7.77		8.46			
	APS1	*Anucleate primary sterigmata protein A*		7.71	8.10			
	Dynein	*Dynein heavy chain*	7.58	7.07	7.49	7.10	7.76	
	ELP1	*Elongator complex protein 1*		7.19	6.89			
	FACT	*FACT complex subunit ctc-1*			7.57	6.47	8.12	7.76
	Helicase	*DNA replication licensing factor mcm3*	7.56	8.03	7.85	7.26	8.00	7.55
	Importin	*Importin subunit beta-3*	7.45	7.33	8.52	7.85	8.54	8.48
	Kinesin 13	*Kinesin class 13; Kinesin heavy chain*	8.37	7.80	8.61	8.38	8.82	8.72
	MAD1	*Spindle assembly checkpoint component MAD1*						
	MAD2	*Mitotic spindle checkpoint component MAD2*						

(*continued on next page*)

Table 3 (*continued*)

	CODE	Protein-Predicted functional partner	Controls		Experiments			
			WT	CYT	γ-TUB	MZT	APS2	SPA10
	MAD3	*Mitotic spindle checkpoint component mad3*						
	met-5	*Homoserine O-acetyltransferase*						
	MTB-3	*Microtubule Binding protein-3*	7.08	7.22	8.71	7.57	8.72	8.88
Microtubules and relevant associated proteins	PrimPol	*DNA primase subunit Pri1*		6.80				
	RFC	*Replication factor C subunit 5*		6.47	7.40			
	SMC-4	*Structural maintenance of chromosomes protein 4*		6.11				
	STU-1	*Protein stu-1*		7.09				
	TBC	*Tubulin-specific chaperone*						
	vATP	*Vacuolar membrane ATPase-6*		7.19	7.42			
	α-Tub (α)	*Tubulin alpha-A chain*	8.59	9.24	9.41	8.95	9.58	9.66
	α-Tub (β)	*Tubulin alpha-B chain*	8.21	9.51	9.65	8.84	9.55	9.68
	β-Tubulin	*Tubulin beta chain*	8.59	9.54	9.73	8.84	9.52	9.89
Septal Intrinsically disordered proteins	SPA1	*Septal pore-associated protein 1*					7.34	
	SPA2	*Septal pore-associated protein 2*		7.89		6.93		
	SPA3	*Septal pore-associated protein 3*		8.62	8.18			7.67
	SPA4	*Septal pore-associated protein 4*						
	SPA5	*Septal pore-associated protein 5*						
	SPA6	*Septal pore-associated protein 6*		8.19	8.09	7.65		7.48
	SPA7	*Septal pore-associated protein 7*		6.63				
	SPA8	*Septal pore-associated protein 8*		7.41				
	SPA9	*Septal pore-associated protein 9*						
	SPA10	***Septal pore-associated protein 10***						8.56
	SPA11	*Septal pore-associated protein 11*	6.37		6.96	6.76		
	SPA12	*Septal pore-associated protein 12*	6.42	7.95	7.25	6.59		8.11
	SPA13	*Septal pore-associated protein 13*						
	SPA14	*Septal pore-associated protein 14*		7.95				
	SPA15	*Septal pore-associated protein 15*	6.27	6.88	7.74	6.51		
	SPA16	*Septal pore-associated protein 16*						
	SPA17	*Septal pore-associated protein 17*						
	SPA18	*Septal pore-associated protein 18*						
Other annotated septa proteins	LIM	*LIM and Rho-GAP domain-containing protein*		6.59	7.40	7.14	7.07	8.11
	Maf/Ham1	*Related to septum formation Maf/Ham1*		7.83	8.93	8.28	8.24	8.32
	PH	*PH domain-containing protein*		7.71	8.10			
	Pkinase_C	*Protein kinase C-like*	7.09		8.28	7.86	8.43	8.39
	RhoGAP	*Rho-GTPase-activating protein 8*	8.21	7.52	8.53	7.80	8.40	8.50
	RhoGEF	*Rho guanyl nucleotide exchange factor*	6.58	6.84	7.82	7.79	8.10	
	sid3	*Related to septum initiation protein sid3*		7.15				

during interphase. However, in repolymerization experiments, we found some evidence for MT nucleation in the cytoplasm, and this activity was apparently independent of γ-tubulin. At septa, we found APS-2, a component generally associated with SPBs, but there was no evidence for the presence of other components of the MTOCs at septa, including γ -tubulin. These findings are in stark contrast to those in *A. nidulans* where septal MTOCs share most of the components with SPBs, and their activities are coordinated through a polo-like kinase (Gao et al., 2021). The question is why the organization of the MT cytoskeleton is so fundamentally different in two related ascomycetous fungi. It has to be considered that *N. crassa* grows very fast with a hyphal extension rate up to 35 μm/min (Collinge and Trinci, 1974), it has a hyphal diameter of ~10 μm and a robust microtubular cytoskeleton (~80 MTs in the first compartment). It can contain ~100 nuclei per compartment (Roper et al., 2011) and mitosis is asynchronous. On the other hand, *A. nidulans* grows at an elongation rate of 2 μm/min, compartments contain 3-6 nuclei, sometimes more in the apical compartment, but not more than 10 (Fischer and Timberlake, 1995), which undergo synchronized mitoses, and the number of MT is less than 10. The 100 nuclei per compartment of *N. crassa* can be translated to 100 SPBs/MTOCs that can initiate the polymerization of at least one cytoplasmic and/or mitotic MT. The microtubular organization does not change significantly when some nuclei undergo mitosis because many cytoplasmic MTs remain. Therefore, at any time, compartments should contain a similarly high

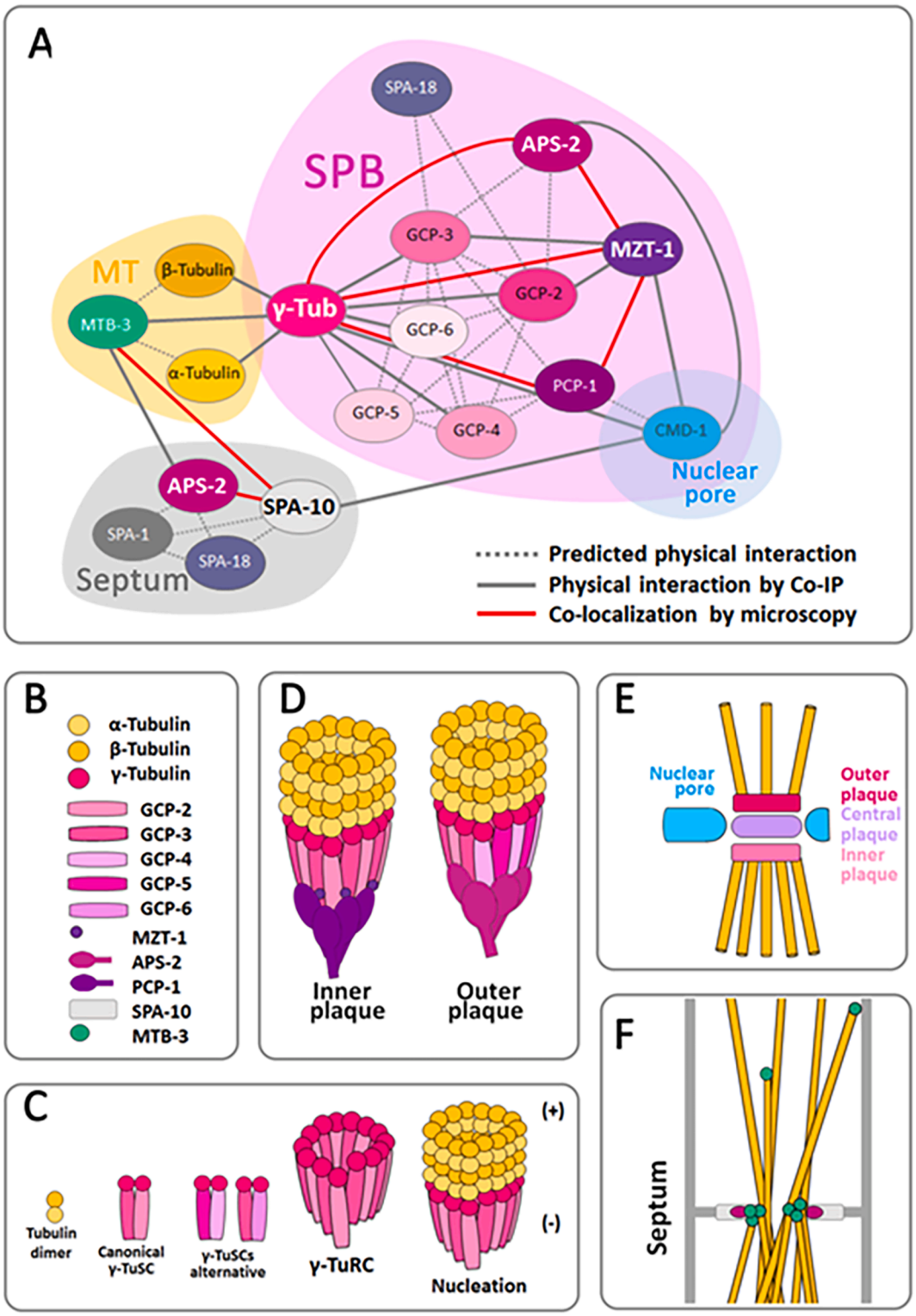

Fig. 9. Model for the *Neurospora crassa* MTOCs. (A) Scheme of the predicted and observe (microscopy and or Co-IP) interaction between MTOC components. (B) Components of the MTOCs. (C) Organization of γ-TuSC and γ-TuRC. (D) MTOCs inner and outer plaque organization. (D) SPB-MTOC organization. (E) Septal MTOC-like organization.

number of MTs, sufficient to support all transport processes, mitoses, or organelle organization. Perhaps this situation creates the need for extra MTOCs obsolete. In *A. nudulans*, with synchronous mitoses (Clutterbuck, 1970; Gladfelter, 2006), cytoplasmic MTs are almost all disassembled, and most MTs are arranged in the mitotic spindles (Riquelme et al., 2003). Septal MTOCs can be a strategy to produce MTs that will support functions different to mitosis. Likewise, a significant difference was also found when fungal hyphae of *N. crassa* or *A. nidulans* grew into channels smaller than the hyphal diameter (Fukuda et al., 2021). Whereas *N. crassa* stopped growth and lost polarity when passing through the channels, *A. nidulans* had no problem resuming normal growth after passing the channels. The differences were attributed to different hyphal

elongation rates (Fukuda et al., 2021).

4.2. Cytoplasmic MT nucleation in the absence of γ-TuRCs

Although there was no evidence for ncMTOCs, we observed MT polymerization in the absence of SPBs and apparently in the absence of γ-tubulin. Recently, it has been proposed that γ-TuRC MT nucleation activity is not enough to support MT *de novo* formation. *In vitro* and *in vivo* evidence suggest that additional processes participate in parallel or synergistically to control MT nucleation (Roostalu and Surrey, 2017). *In vitro* experiments showed spontaneous MT nucleation with the addition of α and β-tubulin dimers in buffer solutions containing GTP and Mg^{2+} ions (Voter and Erickson, 1984). Critical concentrations of α and β-tubulin dimers have been calculated for *in vitro* or *in vivo* MT polymerization, whereas 8 αβ-tubulins are needed as seeds for MT spontaneous nucleation, 4 dimers can nucleate MTs from γ-TuRC. Nevertheless, in pre-assembled MT seeds or an MT "nucleus", a single αβ-tubulin molecule can initiate polymerization (Thawani et al., 2020). There is a drastic reduction of required tubulin ~20 μM for *de novo* nucleation to ~1 μM to support the polymerization of existing MT seeds (Voter and Erickson, 1984; Wieczorek et al., 2015). In *N. crassa*, we found the combination of SPBs/γ-tubulin MTs nucleation and the polymerization of MTs from seeds in the cytoplasm. Similarly, experiments in budding yeast, *Drosophila melanogaster,* and *Physcomitrella patens* revealed a significant number of MTs nucleation events independent of γ-tubulin (Nakaoka et al., 2015; Kitamura et al., 2010; Rogers et al., 2008; Nashchekin et al., 2016). MT nucleation and polymerization are energetically unfavorable processes, and spontaneous polymerization requires one or several MT-stabilizing MTs-associated proteins. The CLIP-associated protein (CLASP), calmodulin-regulated spectrin-associated protein, and $p150^{Glued}$ families have been shown to contribute to microtubule formation independently of the γ-TuRC (Al-Bassam and Chang, 2011). In *N. crassa* the $p150^{Glued}$ subunit of dynactin and the dynein heavy chain were shown to be important for MT nucleation and dynamics (Mouriño-Pérez et al., 2016), comparable to their function in neurons (Lazarus et al., 2013).

4.3. An unorthodox septal Pseudo-MTOC

There was no evidence for a traditional septal MTOCs, although APS-2 and SPA-18, two components of the outer SPB plaque, localized at septa. However, we found an unorthodox novel septal pseudo-MTOC in the septal pore. Still, unlikely the ones associated with SPBs, MT-plus ends were the ones organized through the set of proteins linking MTs to septa. This MTOC does not have the function of MT nucleation but indeed organizes MTs in the septal pore. Those complexes comprised SPA-10, SPA-18, APS-2, and the plus end protein MTB-3. The presence of APS-2 at septa is intriguing, and its function independent of γ-tubulin needs to be addressed. Perhaps it is required for MTB-3 positioning in the septal pore. The novel function of APS-2 at the septum does still not explain the essential function of the protein. The lack of the orthologue in *A. nidulans* causes a reduction in the formation of astral and cytoplasmic MTs (Veith et al., 2005). Since the cytoplasmic MT array solely depends on the activity of the SPBs outer plaques, it would be fatal if the activity of the outer plaques would be severely blocked. If this is the case, the *aps-2* mutant can unfortunately not be tested yet.

Declaration of Competing Interest

The authors declare that they have no known competing financial interests or personal relationships that could have appeared to influence the work reported in this paper.

Data availability

Data will be made available on request.

Acknowledgements

We thank CONACyT and the DFG for the financial support of this work (CONACyT-DFG-2016-277981-RRMP and DFG Fi 459/20-1 (RF)) also for a postdoctoral fellowship grant for RMRC from CONACYT. We are grateful to Dr. Xiaolei Gao at KIT. We thank Lanelle R. Connolly for lab assistance at OSU. Thanks to Dr. Robert Winkler for the advice in the analysis of proteins identified in the Co-IP assays. We acknowledge the Fungal Genetics Stock Center (FGSC, Kansas City, MO) for strains. Thanks to the National Laboratory of Advanced Microscopy of CICESE (LNMA-CICESE) for the support for confocal microscopy observations.

Appendix A. Supplementary data

Supplementary data to this article can be found online at https://doi.org/10.1016/j.fgb.2022.103729.

References

Anders, A., Lourenço, P.C., Sawin, K.E., 2006. Noncore components of the fission yeast gamma-tubulin complex. Mol. Biol. Cell 17, 5075–5093.
Bartolini, F., Gundersen, G.G., 2006. Generation of noncentrosomal microtubule arrays. J. Cell Sci. 119, 4155–4163.
Cavanaugh, A.M., Jaspersen, S.L., 2017. Big lessons from little yeast: budding and fission yeast centrosome structure, duplication, and function. Annu. Rev. Genet. 51 (1), 361–383.
Chabin-Brion, K., Marceiller, J., Perez, F., Settegrana, C., Drechou, A., Durand, G., Poüs, C., Pfeffer, S.R., 2001. The Golgi complex is a microtubule-organizing organelle. Mol. Biol. Cell 12 (7), 2047–2060.
Cota, R.R., Teixidó-Travesa, N., Ezquerra, A., Eibes, S., Lacasa, C., Roig, J., Lüders, J., 2017. MZT1 regulates microtubule nucleation by linking γTuRC assembly to adapter-mediated targeting and activation. J. Cell Sci. 130, 406–419.
Davis, R.H., 2000. Neurospora: contributions of a model organism. Oxford University Press, Oxford, England.
Davis, R.H., Perkins, D.D., 2002. *Neurospora*: a model of model microbes. Nature Rev Genet. 3 (5), 397–403.
Dhani, D.K., Goult, B.T., George, G.M., Rogerson, D.T., Bitton, D.A., Miller, C.J., Schwabe, J.W.R., Tanaka, K., Zheng, Y., 2013. Mzt1/Tam4, a fission yeast MOZART1 homologue, is an essential component of the γ-tubulin complex and directly interacts with GCP3(Alp6). Mol. Biol. Cell 24 (21), 3337–3349.
Fischer, R., Timberlake, W.E., 1995. *Aspergillus nidulans* apsA (anucleate primary sterigmata) encodes a coiled-coil protein required for nuclear positioning and completion of asexual development. J. Cell Biol. 128 (4), 485–498.
Fujita, A., Vardy, L., Garcia, M.A., Toda, T., 2002. A fourth component of the fission yeast gamma-tubulin complex, Alp16, is required for cytoplasmic microtubule integrity and becomes indispensable when gamma-tubulin function is compromised. Mol. Biol. Cell 13, 2360–2373.
Fukuda, S., Yamamoto, R., Yanagisawa, N., Takaya, N., Sato, Y., Riquelme, M., Takeshita, N., Di Pietro, A., 2021. Trade-off between plasticity and velocity in mycelial growth. MBio 12 (2). https://doi.org/10.1128/mBio.03196-20.
Gao, X., Herrero, S., Wernet, V., Erhardt, S., Valerius, O., Braus, G.H., Fischer, R., 2021. The role of *Aspergillus nidulans* polo-like kinase PlkA in microtubule-organizing center control. J. Cell Sci. 134.
Gao, X., Schmid, M., Zhang, Y., Fukuda, S., Takeshita, N., Fischer, R., 2019. The spindle pole body of *Aspergillus nidulans* is asymmetrical and contains changing numbers of γ-tubulin complexes. J. Cell Sci. 132.
Horio, T., Oakley, B.R., 2003. Expression of *Arabidopsis* gamma-tubulin in fission yeast reveals conserved and novel functions of gamma-tubulin. Plant Physiol. 133, 1926–1934.
Horio, T., Uzawa, S., Jung, M.K., Oakley, B.R., Tanaka, K., Yanagida, M., 1991. The fission yeast gamma-tubulin is essential for mitosis and is localized at microtubule organizing centers. J. Cell Sci. 99 (Pt 4), 693–700.
Jaspersen, S.L., Winey, M., 2004. The budding yeast spindle pole body: structure, duplication, and function. Annu. Rev. Cell Dev. Biol. 20 (1), 1–28.
Julian, M., Tollon, Y., Lajoie-Mazenc, I., Moisand, A., Mazarguil, H., Puget, A., Wright, M., 1993. gamma-Tubulin participates in the formation of the midbody during cytokinesis in mammalian cells. J. Cell Sci. 105 (Pt 1), 145–156.
Kaláb, P., Pralle, A., Isacoff, E.Y., Heald, R., Weis, K., 2006. Analysis of a RanGTP-regulated gradient in mitotic somatic cells. Nature 440 (7084), 697–701.
Khodjakov, A., Rieder, C.L., 1999. The sudden recruitment of gamma-tubulin to the centrosome at the onset of mitosis and its dynamic exchange throughout the cell cycle, do not require microtubules. J. Cell Biol. 146, 585–596.
Kilmartin, J.V., 2014. Lessons from yeast: the spindle pole body and the centrosome. Philos. Trans. R. Soc. Lond. B Biol. Sci. 369 (1650), 20130456. https://doi.org/10.1098/rstb.2013.0456.
Knop, M., Schiebel, E., 1997. Spc98p and Spc97p of the yeast gamma-tubulin complex mediate binding to the spindle pole body via their interaction with Spc110p. EMBO J. 16, 6985–6995.

Kollman, J.M., Polka, J.K., Zelter, A., Davis, T.N., Agard, D.A., 2010. Microtubule nucleating gamma-TuSC assembles structures with 13-fold microtubule-like symmetry. Nature 466, 879–882.
Konzack, S., Rischitor, P.E., Enke, C., Fischer, R., 2005. The role of the kinesin motor KipA in microtubule organization and polarized growth of *Aspergillus nidulans*. Mol. Biol. Cell 16 (2), 497–506.
Lajoie-Mazenc, I., Tollon, Y., Detraves, C., Julian, M., Moisand, A., Gueth-Hallonet, C., Debec, A., Salles-Passador, I., Puget, A., Mazarguil, H., et al., 1994. Recruitment of antigenic gamma-tubulin during mitosis in animal cells: presence of gamma-tubulin in the mitotic spindle. J. Cell Sci. 107 (Pt 10), 2825–2837.
Lee, Y.-R., Liu, B.o., 2019. Microtubule nucleation for the assembly of acentrosomal microtubule arrays in plant cells. New Phytol. 222 (4), 1705–1718.
Lin, T.C., Neuner, A., Flemming, D., Liu, P., Chinen, T., Jäkle, U., Arkowitz, R., Schiebel, E., 2016. MOZART1 and γ-tubulin complex receptors are both required to turn γ-TuSC into an active microtubule nucleation template. J. Cell Biol. 215, 823–840.
Lin, T.-C., Neuner, A., Schiebel, E., 2015. Targeting of γ-tubulin complexes to microtubule organizing centers: conservation and divergence. Trends Cell Biol. 25 (5), 296–307.
Lin, T.-C., Neuner, A., Schlosser, Y.T., Scharf, A.ND., Weber, L., Schiebel, E., 2014. Cell-cycle dependent phosphorylation of yeast pericentrin regulates γ-TuSC-mediated microtubule nucleation. Elife. 3.
Liu, B., Joshi, H.C., Wilson, T.J., Silflow, C.D., Palevitz, B.A., Snustad, D.P., 1994. gamma-Tubulin in Arabidopsis: gene sequence, immunoblot, and immunofluorescence studies. Plant Cell 6 (2), 303–314.
Liu, B., Marc, J., Joshi, H.C., Palevitz, B.A., 1993. A gamma-tubulin-related protein associated with the microtubule arrays of higher plants in a cell cycle-dependent manner. J. Cell Sci. 104 (Pt 4), 1217–1228.
Liu, P., Wurtz, M., Zupa, E., Pfeffer, S., Schiebel, E., 2021. Microtubule nucleation: The waltz between gamma-tubulin ring complex and associated proteins. Curr. Opin. Cell Biol. 68, 124–131.
Liu, P., Zupa, E., Neuner, A., Bohler, A., Loerke, J., Flemming, D., Ruppert, T., Rudack, T., Peter, C., Spahn, C., Gruss, O.J., Pfeffer, S., Schiebel, E., 2020. Insights into the assembly and activation of the microtubule nucleator gamma-TuRC. Nature 578, 467–471.
Lynch, E., Groocock, L., Borek, W., Sawin, K., 2014. Activation of the γ-tubulin complex by the Mto1/2 complex. Curr. Biol. 24 (8), 896–903.
Lazarus, J.E., Moughamian, A.J., Tokito, M.K., Holzbaur, E.L.F., 2013. Dynactin Subunit p150Glued Is a Neuron-Specific Anti-Catastrophe Factor. PLoS Biol 11 (7), e1001611. https://doi.org/10.1371/journal.pbio.1001611.
Maia, A.R.R., Zhu, X., Miller, P., Gu, G., Maiato, H., Kaverina, I., 2013. Modulation of Golgi-associated microtubule nucleation throughout the cell cycle. Cytoskeleton (Hoboken). 70 (1), 32–43.
Maiato, H., Rieder, C.L., Khodjakov, A., 2004. Kinetochore-driven formation of kinetochore fibers contributes to spindle assembly during animal mitosis. J. Cell Biol. 167, 831–840.
Masuda, H., Mori, R., Yukawa, M., Toda, T., Zheng, Y., 2013. Fission yeast MOZART1/Mzt1 is an essential γ-tubulin complex component required for complex recruitment to the microtubule organizing center, but not its assembly. Mol. Biol. Cell 24 (18), 2894–2906.
McDaniel, D.P., Roberson, R.W., 1998. γ-Tubulin is a component of the Spitzenkörper and centrosomes in hyphal-tip cells of *Allomyces macrogynus*. Protoplasma. 203 (1-2), 118–123.
Moritz, M., Braunfeld, M.B., Guénebaut, V., Heuser, J., Agard, D.A., 2000. Structure of the gamma-tubulin ring complex: a template for microtubule nucleation. Nat. Cell Biol. 2, 365–370.
Mouriño-Pérez, R.R., Linacre-Rojas, L.P., Román-Gavilanes, A.I., Lew, T.K., Callejas-Negrete, O.A., Roberson, R.W., Freitag, M., Beh, C., 2013. MTB-3, a microtubule plus-end tracking protein (+TIP) of *Neurospora crassa*. PLoS ONE 8 (8), e70655.
Mouriño-Pérez, R.R., Roberson, R.W., Bartnicki-García, S., 2006. Microtubule dynamics and organization during hyphal growth and branching in *Neurospora crassa*. Fungal Genet. Biol. 43 (6), 389–400.
Muresan, V., Joshi, H.C., Besharse, J.C., 1993. Gamma-tubulin in differentiated cell types: localization in the vicinity of basal bodies in retinal photoreceptors and ciliated epithelia. J. Cell Sci. 104 (Pt 4), 1229–1237.
Mouriño-Pérez, R.R., Riquelme, M., Callejas-Negrete, O.A., Galván-Mendoza, J.I., 2016. Microtubules and associated molecular motors in Neurospora crassa. Mycologia 108 (3), 515–527. https://doi.org/10.3852/15-323.
Oakley, B.R., 2004. Tubulins in *Aspergillus nidulans*. Fungal Genet. Biol. 41 (4), 420–427.
Oakley, C.E., Oakley, B.R., 1989. Identification of gamma-tubulin, a new member of the tubulin superfamily encoded by mipA gene of *Aspergillus nidulans*. Nature 338, 662–664.
Paz, J., Lüders, J., 2018. Microtubule-organizing centers: towards a minimal parts list. Trends Cell Biol. 28, 176–187.
Riquelme, M., Fischer, R., Bartnicki-García, S., 2003. Apical growth and mitosis are independent processes in *Aspergillus nidulans*. Protoplasma. 222, 211–215.
Rivero, S., Cardenas, J., Bornens, M., Rios, R.M., 2009. Microtubule nucleation at the cis-side of the Golgi apparatus requires AKAP450 and GM130. EMBO J. 28, 1016–1028.
Roper, M., Ellison, C., Taylor, J.W., Glass, N.L., 2011. Nuclear and genome dynamics in multinucleate ascomycete fungi. Curr. Biol. 21, R786–793.
Roostalu, J., Surrey, T., 2017. Microtubule nucleation: beyond the template. Nat Rev Mol Cell Biol 11, 702–710. https://doi.org/10.1038/nrm.2017.75.
Samejima, I., Miller, V.J., Groocock, L.M., Sawin, K.E., 2008. Two distinct regions of Mto1 are required for normal microtubule nucleation and efficient association with the gamma-tubulin complex in vivo. J. Cell Sci. 121, 3971–3980.
Samejima, I., Miller, V.J., Rincon, S.A., Sawin, K.E., 2010. Fission yeast Mto1 regulates diversity of cytoplasmic microtubule organizing centers. Curr. Biol. 20, 1959–1965.
Snyder, M., 1994. The spindle pole body of yeast. Chromosoma 103, 369–380.
Stearns, T., Evans, L., Kirschner, M., 1991. Gamma-tubulin is a highly conserved component of the centrosome. Cell 65, 825–836.
Straube, A., Brill, M., Oakley, B.R., Horio, T., Steinberg, G., 2003. Microtubule organization requires cell cycle-dependent nucleation at dispersed cytoplasmic sites: polar and perinuclear microtubule organizing centers in the plant pathogen *Ustilago maydis*. Mol. Biol. Cell 14, 642–657.
Teixidó-Travesa, N., Roig, J., Lüders, J., 2012. The where, when and how of microtubule nucleation - one ring to rule them all. J. Cell Sci. 125, 4445–4456.
Uchida, M., Mouriño-Pérez, R.R., Freitag, M., Bartnicki-Garcia, S., Roberson, R.W., 2008. Microtubule dynamics and the role of molecular motors in *Neurospora crassa*. Fungal Genet. Biol. 45, 683–692.
Voter, W.A., Erickson, H.P., 1984. The kinetics of microtubule assembly. Evidence for a two-stage nucleation mechanism. J Biol Chem 259 (16), 10430–10438.
Xiong, Y., Oakley, B.R., 2009. In vivo analysis of the functions of gamma-tubulin-complex proteins. J. Cell Sci. 122, 4218–4227.
Yi, P., Goshima, G., 2018. Microtubule nucleation and organization without centrosomes. Curr. Opin. Plant Biol. 46, 1–7.
Zekert, N., Veith, D., Fischer, R., 2010. Interaction of the *Aspergillus nidulans* microtubule-organizing center (MTOC) component ApsB with gamma-tubulin and evidence for a role of a subclass of peroxisomes in the formation of septal MTOCs. Eukaryot. Cell 9, 795–805.
Zhang, Y., Gao, X., Manck, R., Schmid, M., Osmani, A.H., Osmani, S.A., Takeshita, N., Fischer, R., 2017. Microtubule-organizing centers of *Aspergillus nidulans* are anchored at septa by a disordered protein. Mol. Microbiol. 106, 285–303.
Zheng, Y., Jung, M.K., Oakley, B.R., 1991. Gamma-tubulin is present in *Drosophila melanogaster* and *Homo sapiens* and is associated with the centrosome. Cell 65, 817–823.
Zimmerman, W.C., Sillibourne, J., Rosa, J., Doxsey, S.J., 2004. Mitosis-specific anchoring of gamma tubulin complexes by pericentrin controls spindle organization and mitotic entry. Mol. Biol. Cell 15, 3642–3657.
Zupa, E., Liu, P., Wurtz, M., Schiebel, E., Pfeffer, S., 2021. The structure of the gamma-TuRC: a 25-years-old molecular puzzle. Curr. Opin. Struct. Biol. 66, 15–21.